IEEE Access
Multidisciplinary ⋮ Rapid Review ⋮ Open Access Journal

Received 1 December 2022, accepted 26 December 2022, date of publication 27 December 2022, date of current version 3 January 2023.

Digital Object Identifier 10.1109/ACCESS.2022.3232729

TOPICAL REVIEW

Applications of the Generalized Morse Wavelets: A Review

ERICK AXEL MARTINEZ-RÍOS[1], ROGELIO BUSTAMANTE-BELLO[1], SERGIO NAVARRO-TUCH[1], (Member, IEEE), AND HECTOR PEREZ-MEANA[2], (Life Senior Member, IEEE)

[1]School of Engineering and Sciences, Tecnologico de Monterrey, Mexico City 14380, Mexico
[2]ESIME Culhuacan, Instituto Politecnico Nacional, Mexico City 04260, Mexico

Corresponding author: Erick Axel Martinez-Ríos (a01331212@tec.mx)

The work of Erick Axel Martinez-Ríos was supported by the Scholarship awarded by the Tecnologico de Monterrey and Consejo Nacional de Ciencia y Tecnologia through the Currículum Vitae Único (CVU) under Grant 1010770.

ABSTRACT The study of signals, processes, and systems has motivated the development of different representations that can be used to analyze and understand them. Classical ways of studying the behavior of signals are the time domain and frequency domain representations. For the analysis of non-stationary signals, time-frequency representations have become an essential tool to understand how the frequency content of signals changes with time. A common time-frequency technique employed in the literature is the wavelet transform. Nevertheless, selecting an adequate mother wavelet to perform the wavelet transform has become challenging due to the diverse available wavelet families. This paper reviews the applications and uses of a particular class of wavelet basis known as the Generalized Morse Wavelets. This class of wavelet family provides a systematic framework to choose and generate a wavelet for general-purpose use. This study reviews the application of Generalized Morse Wavelets in biomedical engineering, dynamical systems analysis, electrical engineering, geophysics, and communication systems. Moreover, the parameters of the Generalized Morse Wavelets used in each study are presented. The results of this study reveal that Generalized Morse Wavelets have proven helpful in studying signals, systems, and processes in areas ranging from biomedical engineering to geophysics. Nonetheless, the parameters of the Generalized Morse Wavelets are yet to be chosen through a rigorous methodology and argumentation. Therefore, there is an opportunity to generate methods for selecting the parameters of the Generalized Morse Wavelets based on the characteristics of the signals, systems, or processes under research.

INDEX TERMS Generalized Morse wavelets, mother wavelet selection, continuous wavelet transform, applications, time-frequency analysis.

I. INTRODUCTION

The analysis of signals can be performed in three general frameworks, the time domain, the frequency domain, and the so-called time-frequency domain. The time domain analysis studies the signal's amplitude that changes over time. On the other hand, frequency analysis is concerned with the spectral content of the signal obtained through the Fourier transform. In the case of time-frequency analysis, this framework is interested in the signal processing methods, techniques, and algorithms that help quantify a signal's spectral content over time. In the framework of time-frequency analysis, the natural variables known as time (t) and frequency (f) are used concurrently [1]. Contrary to classical signal processing techniques like the Fourier transform, where the frequency is analyzed independently of time or a signal defined in the time domain does not provide information about its frequency content.

In this way, time-frequency analysis provides a set of methods to capture a signal's time and frequency content through a 2D representation that simultaneously provides both time and frequency localization. Thus, this paradigm

The associate editor coordinating the review of this manuscript and approving it for publication was Jiafeng Xie.

constitutes a crucial tool for studying non-stationary signals (i.e., signals whose statistics change with time [2]). As a result, the study of non-stationary signals has developed techniques such as the Short-Time Fourier Transform (STFT) or Gabor Transform, Wigner–Ville Distribution (WVD), Hilbert-Huang Transform (HHT) and Wavelet Transform (WT) [3]. Particularly, the WT can be understood as a generalization of the Fourier transform; the main difference is that in the case of the Fourier transform, the decomposition is made through complex exponentials, and in the case of the WT, the decomposition is performed through the so-called wavelet functions [4].

This set of techniques has gained popularity in diverse fields such as mechanics, geophysics, electrical engineering, communication systems, medical, and compression tasks [5], [6], [7]. More recently, time-frequency methods have been used as signal representation techniques in combination with machine learning or deep learning techniques to solve classification problems in a diverse set of applications [8]. For example, biomedical signal processing has been one of the fields that have adopted extensively time-frequency analysis techniques for health monitoring applications or to perform diagnosis [9], [10]. Furthermore, in the case of power systems, time-frequency methods have also been used to monitor or detect faults in electrical components such as batteries, motors, capacitors, or power inverters [11], [12].

Despite the widespread use of time-frequency methods in different areas, one of the main challenges that time-frequency analysis imposes is selecting an appropriate tool to represent the time and frequency content of the signal correctly. This is because there is yet to be an exact method to verify that the obtained representation is adequate for a particular signal or problem [1]. The above is also influenced due to Heisenberg's uncertainty principle, also known as the Heisenberg-Gabor uncertainty principle or Gabor Limit [13]. This principle states that a function cannot simultaneously be arbitrarily compact in time and frequency [14].

The above implies that it is challenging to localize finite oscillations transients simultaneously in time and frequency [13]. For instance, the STFT provides a time-frequency representation but with a fixed resolution in the time and frequency domains since the transform depends on the setting of a fixed window length [15]. In the case of the WT, this challenge is related to determining an adequate type of mother wavelet that will be used to decompose the signal [16].

Different mother wavelets have been proposed in the literature, such as the Morlet, Daubechies, Derivative of Gaussian, Bessel, Mexican Hat, Meyer, and Shannon wavelets [17], [18], [19]. Nevertheless, these diverse sets of wavelet types and the various time-frequency methods have imposed the challenge of selecting one for a particular application. Therefore, a common approach in the literature is to test different wavelet types to choose one for a specific problem [18]. Moreover, according to the review presented by Guo et al. [19], a systematic method that allows the selection of an optimal wavelet basis and its evaluation is still required to convey applications based on the WT and derived techniques.

The above challenges motivated the work of Lilly et al. [18], which introduced the Generalized Morse Wavelets (GMWs), a superfamily of analytic wavelets that provides a systematic and unified framework to understand the analytic wavelet functions and their properties. Daubechies and Paul initially presented GMWs in [20] as eigenfunctions of a time-frequency operator and were further studied in [21]. GMWs unify in single-family different families of wavelets such as lognormal wavelets, Airy wavelets, Cauchy wavelets, the Shannon wavelet, and even complex exponentials. These characteristics make GMWs a recommended starting point for general-purpose use [18].

Recent studies have presented literature reviews on the use of the WT and its applications. These studies either investigate the applications of the WT in a diverse set of fields or for particular applications. For instance, the study of Rhif et al. [16] showed the applications of the WT and derived techniques in the fields of geosciences and geophysics, engineering, hydrology, finance, medicine, and remote sensing for analyzing vegetation. Furthermore, Wang et al. [22] presented a study focused on the HHT and WT applications in the structural engineering field. In [23], the Tunable Q-factor Wavelet Transform (TQWT) implementations related to fault diagnosis on rolling element bearing were reviewed. Camussi et al. [24] presented the uses of the WT in aeroacoustics, emphasizing the study of compressible jets. Rinoshika et al. [25] showed the implementations of multi-dimensional orthogonal WT in fluid mechanics, particularly turbulent wakes and turbulent boundary layer flows were reviewed. Nevertheless, few studies have analyzed the particular use of certain wavelet families or mother wavelets and how they have been used and parameterized for particular signals, systems, and processes.

This paper presents a review of the applications of GMWs. This study aims to provide an overview and discussion on the uses of GMWs in different fields and how they have been parameterized for particular signals, systems, and processes. Furthermore, the implications of the parametrizations selected for each application are also explored and discussed. The applications were divided into the following fields: medical and biomedical engineering, fluid dynamics, vibrations analysis, systems analysis, electrical engineering, geophysics, and communications systems. Fig. 1 presents a general overview of the structure of this study. The main contributions of this study are outlined as follows.

- A summary of the Generalized Morse Wavelets applications is presented related to biomedical engineering, dynamical systems analysis, electrical engineering, geophysics, and communication systems.
- The parametrizations of the Generalized Morse Wavelets employed for analyzing or performing each reviewed application and field are summarized.
- A detailed analysis and discussion of the values of the parameters that have been used to perform the

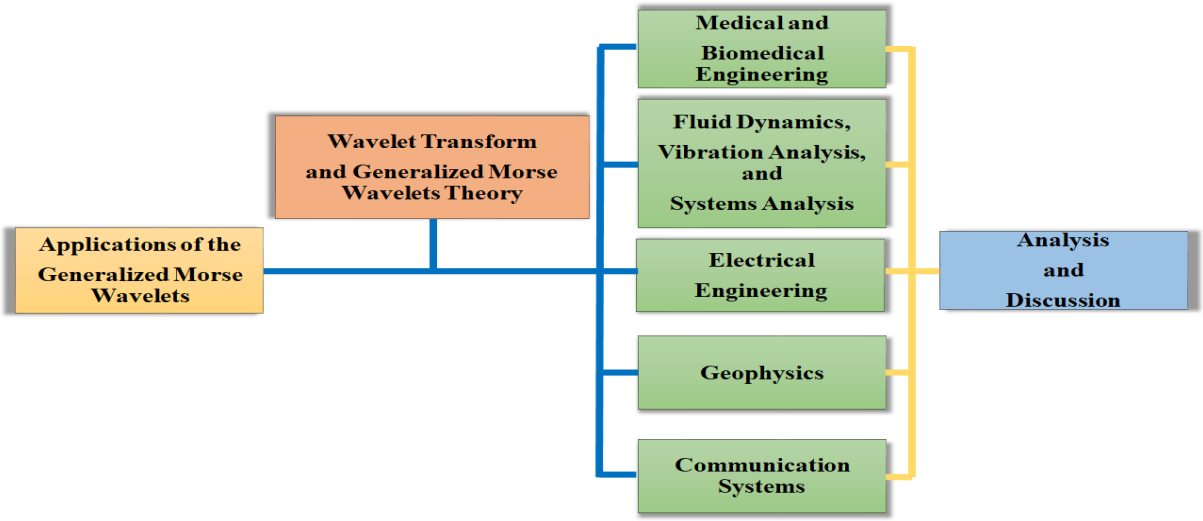

FIGURE 1. The outline of the structure of this review concentrated on the applications of the Generalized Morse Wavelets. First, the theoretical background of the wavelet transform and Generalized Morse Wavelets is presented. The review of the applications of Morse wavelets in medical and biomedical engineering, fluid dynamics, vibration analysis, systems analysis, electrical engineering, geophysics, and communications systems is presented. The last section of this study corresponds to the analysis and discussion of the results.

continuous wavelet transform through the Generalized Morse Wavelets are presented.

The remainder of this study is organized as follows. Section II explains the search strategy and selection criteria for developing this review. Section III presents an overview of the theoretical background of the WT and GMWs. Section IV shows a summary of the applications of the GMWs with their corresponding parametrizations and analyzed signal, system, or process. The discussion is presented in Section V while Section VI explains the limitations of this review. Finally, Section VII presents the conclusions and future research directions related to utilizing GMWs.

II. SEARCH STRATEGY AND SELECTION CRITERIA

The journal and conference articles were searched for this review from 2013 to 2022. This search was primarily based on the Web of Science and Scopus databases. The main keywords used to perform the search in this study are listed below.

- Time-Frequency Analysis;
- Wavelet Transform;
- Continuous Wavelet Transform;
- Generalized Morse Wavelets;
- Applications.

The inclusion of articles was based on the use of GMWs. The articles were discarded if the GMWs were only mentioned but not used in the referred study or its methodology. Based on these criteria, the selected articles were classified into the following fields; mainly biomedical engineering, dynamical systems analysis (i.e., fluid dynamics, vibration analysis, and general use in systems analysis), electrical engineering, geophysics, and communication systems. The critical information extracted from each publication was the author's name, year of publication, parametrization of the GMWs used in the study, type of analyzed processes, signals or systems studied via the CWT and GMWs, and the overall application performed in the study that was selected. Contrary to previous reviews that have focused on the WT applications in different fields such as the one presented by Guo et al. [19], this study mainly focuses on the applications of WT and CWT generated through the so-called GMWs and their parameters.

III. WAVELET TRANSFORM AND GENERALIZED MORSE WAVELETS

This section presents a brief overview of the WT and GMWs. This is done to provide the general theoretical background that defines the methods reviewed in this literature review.

A. WAVELET TRANSFORM

The concept of the WT was first formalized by the work of Morlet et al. [5] while analyzing seismic data, and the wavelets' mathematical support was described in [26]. The WT expands the concept of the Fourier transform to a general class of orthogonal basis and partially overcomes Heisenberg's uncertainty principle by performing a multi-resolution decomposition as appreciated in Fig. 2 [4]. This multi-resolution method allows obtaining various temporal and frequency resolutions in different frequency bands, which help break down complicated signals produced by multi-scale processes. Fig. 2a illustrates the resolution of the time domain representation, while Fig. 2b shows the frequency domain resolution. Fig. 2c shows the resolution of the STFT's spectrogram. Notice that this resolution is fixed according to the window's length despite having a resolution in the time and frequency domains. The WT counters this problem by allowing multiple window lengths as illustrated in Fig. 2d.

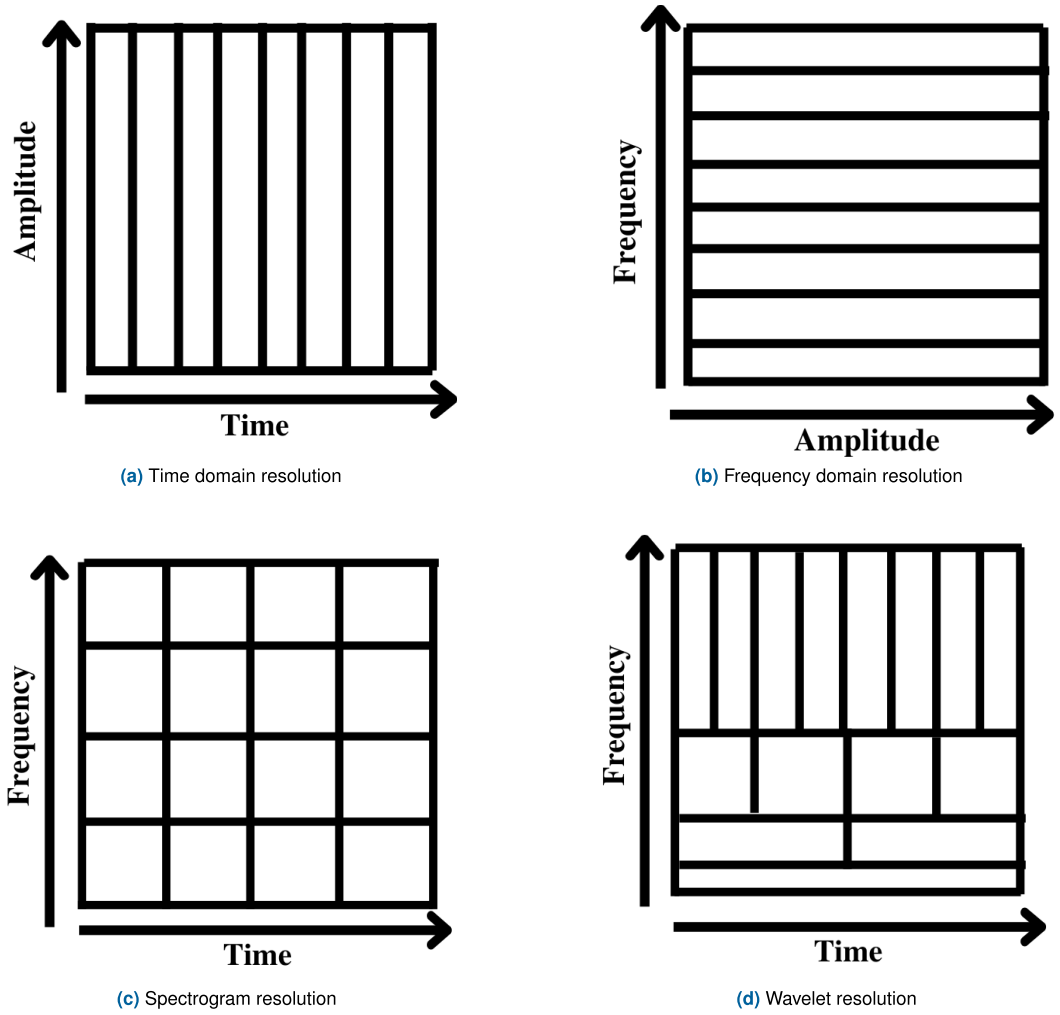

(a) Time domain resolution

(b) Frequency domain resolution

(c) Spectrogram resolution

(d) Wavelet resolution

FIGURE 2. Illustration of resolution limitations and uncertainty in the time domain, frequency domain, Short-Time Fourier Transform or spectrogram, and multi-resolution analysis performed through the Wavelet Transform. a) Shows the time domain resolution, b) Shows the frequency domain resolution, c) Shows the spectrogram resolution, d) Shows the multi-resolution decomposition computed through the wavelet transform.

The WT decomposes a signal with the usage of translated and dilated wavelets. A wavelet is a square-integrable function ($\psi \in L^2(\mathbb{R})$) that has zero mean as shown in (1) [27].

$$\int_{-\infty}^{\infty} \psi(t)dt = 0 \tag{1}$$

Moreover, this wavelet function is normalized ($\|\psi\| = 1$) and centered at $t = 0$.

Additionally, the wavelet must satisfy the admissibility condition, as shown in (2). The term $\Psi(\omega)$ is the Fourier transform of the wavelet $\psi(t)$.

$$\int_{-\infty}^{\infty} \frac{|\Psi(\omega)|^2}{|\omega|} d\omega < \infty \tag{2}$$

The admissibility criterion allows obtaining an invertible and stable transform [28]. Moreover, this condition shows that the wavelet must oscillate and decay. To assure that the integral presented in (2) is finite, the mean of the function must be zero as presented in (1). The above explains why a wavelet must have a zero mean.

By translating and scaling the wavelet function by factors (u) and (s), respectively, a dictionary (D) of wavelet functions is obtained as shown in (3) [27].

$$\mathrm{D} = \left\{ \psi_{u,s}(t) = \frac{1}{\sqrt{s}} \psi\left(\frac{t-u}{s}\right) \right\}_{u\in\mathbb{R}, s\in\mathbb{R}^+} \tag{3}$$

The term $\frac{1}{\sqrt{s}}$ normalizes the energy of the decomposition across the scales (s).

These wavelets remain normalized $\|\psi_{u,s}\| = 1$. Consequently, the WT of a square-integrable function ($f \in L^2(\mathbb{R})$) at time (u) and scale (s) is given in (4) [27]. The asterisk indicates the complex conjugate.

$$Wf(u,s) = \langle f(t), \psi_{u,s}(t) \rangle = \int_{-\infty}^{\infty} f(t) \frac{1}{\sqrt{s}} \psi^*\left(\frac{t-u}{s}\right) dt \tag{4}$$

The coefficients computed through (4), also named wavelet coefficients, represent the degree of similarity or correlation between $f(t)$ and the wavelet $\psi_{u,s}(t)$ at a particular translation (u) and a specific scale (s). Furthermore, the WT can be expressed as a convolution product as shown in (5) [27].

$$Wf(u,s) = \int_{-\infty}^{\infty} f(t)\frac{1}{\sqrt{s}}\psi^*(\frac{t-u}{s})dt = f \star \overline{\psi}_s(u) \tag{5}$$

with

$$\overline{\psi}_s(t) = \frac{1}{\sqrt{s}}\psi^*(\frac{-t}{s}) \tag{6}$$

Moreover, the Fourier transform of $\overline{\psi}_s(t)$ is expressed in (7).

$$\widehat{\overline{\psi}_s}(\omega) = \sqrt{s}\widehat{\psi^*}(s\omega) \tag{7}$$

The above suggests that the WT exhibits a linear filtering operation on the function $f(t)$ for each frequency scale. Since $\widehat{\psi}(0) = \int_{-\infty}^{\infty}\psi(t)dt = 0$, it seems that $\widehat{\psi}$ is equivalent to the transfer function of band-pass filters. Thus, the filters generated by scaling ψ, also known as the mother wavelet, are bandpass filters. Therefore, the convolution of the WT computes the transformation with dilated bandpass filters. The information at different scales is obtained by scaling the mother wavelet and convolving the scaled wavelet with the analyzed signal. The mother wavelet captures the highest frequency from the signal, while the scaled wavelets will capture the information at lower frequencies [27].

Moreover, the WT will exhibit a better time resolution at high frequencies but a lower frequency resolution. Otherwise, at lower frequencies, the wavelet will have a better frequency resolution but a lower time resolution. The above is illustrated in Fig. 2d.

The term continuous wavelet transform (CWT) refers that the scale (s), and translation (u) parameters shown in (5) are varied continuously rather than to a continuous time function. Otherwise, the discrete wavelet transform employs what is called dyadic sampling to choose the values of the scale and translation parameters. The dyadic sampling process involves selecting values equal to the powers of two. The above can be expressed as shown in (8) where j is the scale parameter, and k is the shift parameter, both of which are integers.

$$\psi_{j,k}(t) = \frac{1}{\sqrt{2^j}}\psi(\frac{t-k2^j}{2^j}) \tag{8}$$

In addition, with the adequate selection of a wavelet, the discrete wavelet transform could produce an orthogonal basis (e.g., Meyer wavelet or Daubechies wavelets). The above makes the discrete wavelet transform a common choice for audio or image compression tasks [27]. In this case, the GMWs are mostly used through the CWT rather than the discrete wavelet transform. This wavelet family will be introduced in the following section.

B. GENERALIZED MORSE WAVELETS

This section presents a general overview of the theoretical background of GMWs and their properties. Nevertheless, a deeper explanation of this wavelet family can be found in [18], [21], and [30].

GMWs are time-frequency localized filters with vanishing support at negative frequencies, making them analytical functions. Although an analytical function must necessarily be complex, they are entirely characterized by its real part. Analytical wavelets are preferred to analyze the oscillatory behavior of signals or time evolution of frequency transients [27]. The above is achieved by decoupling the amplitude and phase of the signal through complex functions. On the other hand, real or non-analytical wavelets are better suited to localized discontinuities or sharp signal transitions [18], [27]. GMWs are expressed in the frequency domain as shown in (9).

$$\Psi_{\beta,\gamma} = \int_{-\infty}^{\infty}\psi_{\beta,\gamma}(t)e^{-i\omega t}dt = U(\omega)a_{\beta,\gamma}\omega^{\beta}e^{-\omega^{\gamma}} \tag{9}$$

where $\Psi_{\beta,\gamma}$ is the frequency domain representation of the GMWs, $\psi_{\beta,\gamma}(t)$ is the time domain wavelet function, $a_{\beta,\gamma}$ is a normalization constant, $U(\omega)$ represents a unit step function defined in the frequency domain, β and γ are the parameters that control the wavelet form. The parameters β and γ control the wavelet function's time and frequency domain decay, respectively. To be a valid wavelet, the gamma and beta must be greater than zero ($\gamma > 0, \beta > 0$). The normalization constant is equivalent to $a_{\beta,\gamma} \equiv 2(e\gamma/\beta)^{\beta/\gamma}$ with e being Euler's number [30]. In addition, the frequency domain representation of the GMWs achieved their maximum value at the peak frequency $\omega_{\beta,\gamma} \equiv (\frac{\beta}{\gamma})^{1/\gamma}$. This is the frequency at which the derivative of $\Psi_{\beta,\gamma}(\omega)$ with respect to ω becomes zero [31].

GMWs receive their name since, by considering $\gamma = 1$, this family of wavelets is equivalent to a solution of the Schrödinger equation studied by Morse in [32]. Furthermore, the selection of a wavelet is reduced to selecting the values of β and γ in this super-family of wavelets.

The parameter space of the GMWs can be set based on the Heisenberg Area, a measurement of the time-frequency concentration and energy localization of a wavelet. The Heisenberg area is defined as shown in (10). Where σ_t and σ_ω are the standard deviation of the wavelet in the time and frequency domains, respectively. Hence, the setting of β and γ provides a way to control the wavelet function's form in time and frequency. For fixed values of γ and increasing values of β, Heisenberg's area of GMWs decreases [18].

$$A_\psi \equiv \sigma_t\sigma_\omega \tag{10}$$

Furthermore, based on Heisenberg's uncertainty principle, it is known that Heisenberg's area is at least one-half as expressed in (11) [27].

$$\sigma_t\sigma_\omega \geq \frac{1}{2} \tag{11}$$

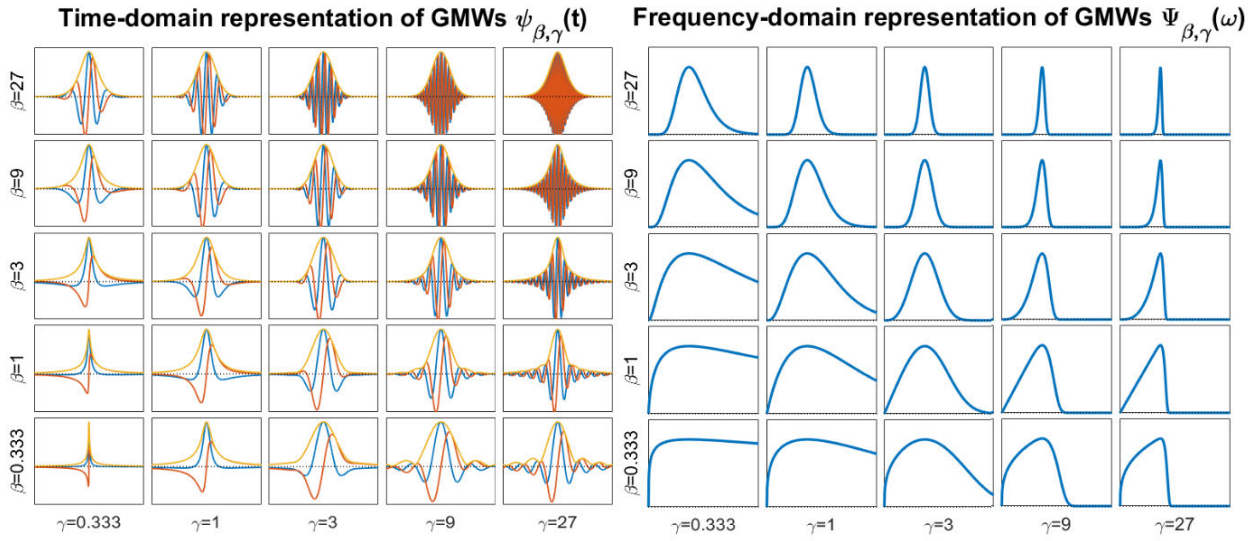

FIGURE 3. Time and frequency domain representations of the Generalized Morse Wavelets for different values of gamma and beta. The left section shows the time domain representation of the Generalized Morse Wavelets. The blue function represents the real part of the wavelet, the orange function is the imaginary part of the wavelet, and the yellow function represents the magnitude of the wavelet function. The right section shows the magnitude of the Fourier transform of the Generalized Morse Wavelets. This image was adapted from [18] with the help of the software package provided in [29].

This lower-bound is achieved by Gaussian functions of the form shown in (12) for $\alpha > 0$, and ρ is a constant [33].

$$\psi(t) = \rho e^{-\alpha(t-t_0)^2 + j\omega_0 t} \tag{12}$$

In the case of GMWs, Heisenberg's area lower-bound is achieved for $\gamma = 3$, which is equivalent to the so-called Airy wavelets. These wavelets are the most symmetrical and most nearly Gaussian [18]. Besides, the Heisenberg area is undefined for $\beta \leq \frac{1}{2}$. Additionally, the dimensionless duration of the wavelet in the time domain or inverse bandwidth can be defined in terms of β and γ as shown in (13). The $P_{\beta,\gamma}$ term allows controlling the number of oscillations of the wavelet in the time domain.

$$P_{\beta,\gamma} = \sqrt{\beta\gamma} \tag{13}$$

GMWs can be expressed in terms of the duration $P_{\beta,\gamma}$, which leads to the expression shown in (14):

$$\Psi_{P,\gamma} = \int_{-\infty}^{\infty} \psi_{P,\gamma}(t) e^{-i\omega t} dt = U(\omega) a_{P,\gamma} \omega^{\frac{P^2}{\gamma}} e^{-\omega^{\gamma}} \tag{14}$$

The expression shown in (13) when expressed as shown in (15) receives the name of the time-bandwidth product.

$$P^2 = \beta\gamma \tag{15}$$

Other families of wavelets that can be obtained by changing the values of γ are the Derivative of Gaussian family for $\gamma = 2$ and the Cauchy family for $\gamma = 1$. As mentioned before, when $\gamma = 3$, the GMWs are equivalent to the Airy Wavelets, which are approximately equal to the Morlet Wavelets. Nevertheless, Morlet Wavelets are not strictly analytical as presented in [18]. Therefore, GMWs, by being analytical, avoid problems associated with non-analytical wavelets, such as the introduction of artifacts and interference in the time-frequency plane, which yields erroneous amplitude and phase estimates [31].

In addition, as stated in [30], GMWs only have a finite time spread for $\beta > \frac{1}{2}$. Having a very long time decay is useless in practice. Thus, a lower-bound can be set at $\beta = 1$ for useful values of β as explained by Lilly et al. [30]. On the other hand, the smallest value of the duration parameters $P_{\beta,\gamma}$ is at $P_{\beta,\gamma} = 1$; this implies that $\gamma = 1$. The above suggests that the wavelet completes a full cycle within its central window.

Finally, Fig. 3 shows the behavior of the GMWs in the time (see Fig. 3 left) and frequency (see Fig. 3 right) domains for different values of γ and β. In general, by examining Fig. 3 it is possible to notice that by increasing the value of β and fixing the value of γ, the number of oscillations and thus the time duration of the wavelet increases. On the other hand, when the value of γ increases or decreases and the values of β remain constant, the symmetry of the frequency representation changes. By increasing γ, the skewness of the frequency representation becomes negative. Otherwise, by decreasing γ, the skewness becomes positive [18].

C. SOFTWARE IMPLEMENTATIONS OF THE GENERALIZED MORSE WAVELETS

The software implementation of GMWs is provided by Lilly et al. [29] in the data analysis package for MATLAB named jLab. Specifically, the jWavelet module of the jLab package provides functions to compute the CWT, the

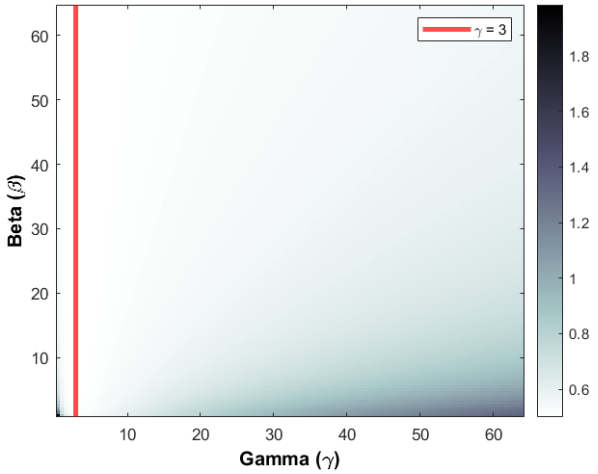

FIGURE 4. Heisenberg area of the parameter space of the Generalized Morse Wavelets. The darker tones correspond to a higher Heisenberg Area, while the whiter colors refer to a lower Heisenberg area. It is essential to highlight that the value of the Heisenberg area has a lower-bound of one-half; therefore, the color scale has a lower-bound of 0.5. The vertical red line denotes the gamma value of 3, where the Generalized Morse Wavelets approximate the lower-bound of the Heisenberg Area.

Heisenberg area and Heisenberg box of the GMWs, the frequency domain derivatives of GMWs, and the Morlet wavelet can be computed for comparison with the GMWs. On the other hand, the MATLAB implementation of the CWT uses the GMW family to compute the WT coefficients. The parameterization used in the MATLAB implementation is equivalent to the one shown in (14); thus, two parameters are set gamma (γ) and the time-bandwidth product (P^2). The default value of gamma is $\gamma = 3$, while the default value of the time-bandwidth product is $P^2 = 60$. Notice that the value of gamma is not set arbitrarily in the MATLAB implementation since, as mentioned in the previous Section, GMWs exhibit a zero skewness for $\gamma = 3$ and achieve the lower-bound of the Heisenberg's area presented in (11).

Fig. 4 shows Heisenberg's area of the GMWs computed through the help of the jLab package provided in [29]. The Heisenberg's area shown in Fig. 4 was concentrated in values of beta greater than one-half since the area is under-defined for values smaller or equal to one-half. Hence, the beta values are from the range of 1 to 64. Otherwise, the values of gamma were between one-half and 64. The darker colors shown in Fig. 4 correspond to a greater Heisenberg area, while the whiter colors correspond to a lower Heisenberg area. As explained in the previous Section, the lower-bound of the Heisenberg area is 0.5. Therefore, the vertical red line denotes the value of $\gamma = 3$, where GMWs approximates Heisenberg's area lower-bound.

IV. APPLICATIONS OF THE GENERALIZED MORSE WAVELETS

A. MEDICAL AND BIOMEDICAL ENGINEERING APPLICATIONS

Time-frequency analysis has been applied extensively to analyze and classify physiological signals. Electrocardiography (ECG), electromyography (EMG), photoplethysmography (PPG), electrooculography (EOG), and electroencephalography (EEG) are examples of physiological signals that have been studied in biomedical and medical engineering applications. The above is done since physiological signals are considered non-stationary phenomena [34], [35], [36], [37], [38]. Within the literature, the applications of GMWs have been focused on two main applications, disease detection or physiological signal classification. Table 1 shows a summary of the studies and the parametrizations of the GMWs used in medical and biomedical engineering applications. The parameters of the GMWs under parenthesis in Table 1 were estimated based on the expression shown in (13); nevertheless, they were not initially reported by the authors of the respective study.

One recent example of the use of GMWs in the field of biomedical engineering and disease detection is the work of Yan et al. [34], where low dimensional spectro-temporal features were used for seizure detection. The spectro-temporal features were derived from EEG data through the CWT. The mother wavelet was a Morse wavelet with the default parameters available in the MATLAB implementation, which takes a gamma value of $\gamma = 3$ and a time-bandwidth product of $P^2 = 60$. In addition, this representation used the mean-standard deviation of the WT coefficients as features. Finally, the detection was performed with a 1D convolutional neural network (CNN).

Likewise, Mohanto et al. [46] proposed using the CWT and Morse wavelet for arrhythmia detection performed through a 2D CNN. The trained model was used to detect five types of heartbeats by processing ECG data: normal, left bundle branch block, right bundle branch block, atrial premature, and premature ventricular contraction. However, the parameters of the Morse wavelet were not specified by the authors. Furthermore, in [45], GMWs were used for abnormal heart sound classification in combination with CNNs. Nevertheless, similar to Mohanto's study, the parameters of the Morse wavelet were not conveyed.

Alafeef et al. [39] proposed a gait analysis system to diagnose idiopathic Parkinson's disease. The methodology consisted in computing the CWT of the vertical ground reaction force through a Morse wavelet and plotting the real value and imaginary part of the CWT coefficients. Based on the generated plot, the area of the generated ellipse shape was estimated and used as a feature, along with the CWT's mean and peak energy. The classification was performed through the use of an artificial neural network. This work set gamma to 3, and the time-bandwidth product was designated to 60. These values coincide with the default values established by the MATLAB implementation of the GMWs and the CWT.

GMWs have also been used on physiological signals for the analysis of stress. For instance, in [47], the skin potential response (SPR) signals measured from the hands of the drivers and the ECG were used to evaluate the presence of stress intervals in traffic and nontraffic scenarios. In particular, the CWT performed with the help of a Morse wavelet

TABLE 1. Summary of the parametrizations used for Generalized Morse Wavelets in medical and biomedical engineer applications.

Author	Year	Parameters of GMWs	Analyzed signal, system, or process	Application of the GMW
Wachowiak et al. [37]	2018	$\gamma = 3, \beta = 8$ $(P^2 = 24)$	EMG signal	Isolation of relevant features from EMG in muscle bursts while skating and assessing heart variability through ECG.
		$\gamma = 3, \beta = 4$ $(P^2 = 12)$	ECG signal	
Alafeef et al. [39]	2019	$\gamma = 3, P^2 = 60$ $(\beta = 20)$	Vertical Ground Reaction Force	Diagnosis of idiopathic Parkinson's disease.
Byeon et al. [40]	2019	$\gamma = 3, P^2 = 60$ $(\beta = 20)$	ECG signal	Biometric identification through ECG.
Cartas-Rosado et al. [41]	2020	$\gamma = 3, P^2 = 60$ $(\beta = 20)$	ECG signal	Analysis of heart rate variability and estimation of the autonomic cardiac regulation.
Smarr et al. [42]	2020	$\gamma = 3, \beta = 5$ $(P^2 = 15)$	Temperature time series data	Analysis of temperature data through the CWT.
Grant et al. [43]	2020	$\gamma = 3, \beta = 5$ $(P^2 = 15)$	Data related to high frequency distal body temperature, the sleeping heart rate, the sleeping heart rate variability, and the sleep timing.	Prediction of the preovulatory luteinizing hormone.
Wiklendt et al. [44]	2020	$\gamma = 3, \beta = 1.58174$ $(P^2 = 4.74522)$	Synthetic signals and EMG data	Filtering of frequencies related to the shape of action potentials in electrophysiology.
Malik et al. [45]	2020	Not reported	Heart sound audio data	Classification of abnormal heart sounds through CNNs.
Agarwal et al. [36]	2022	Not reported	EEG data	Imagined speech recognition performed through CWT and CNN
Yan et al. [34]	2022	$\gamma = 3, P^2 = 60$ $(\beta = 20)$	EEG signal	Extraction of spectro-temporal features for Seizure detection.
Mohonta et al. [46]	2022	Not reported	ECG signal	Arrhythmia classification through CWT and CNNs.
Zontone et al. [47]	2022	$\gamma = 3, P^2 = 60,$ $(\beta = 20)$	Skin Potential Response signals	Stress interval analysis by measuring SPR and employing the CWT.
Campi et al. [48]	2022	Not reported	Daily deaths and RIC-index data	Analysis of the epidemic evolution of COVID-19 through daily deaths and RIC-index data.
Davila et al. [49]	2022	$\gamma = 3, P^2 = 60$ $(\beta = 20)$	EEG data	Estimation of the root-mean-square gamma power through a CWT filter bank.

was used to analyze the SPR signals and identify patterns that show intervals of stress. The ECG and EMG were also investigated in [37] by applying the GMWs. These wavelets were used to isolate relevant features from EMG in muscle bursts while skating and assess heart variability in the ECG. The parameters of the Morse wavelet to generate the scalogram for the EMG signal were $\beta = 8$, and $\gamma = 3$, and for the ECG signal, were $\beta = 4$, and $\gamma = 3$. Another example of the analysis of ECG data through Morse wavelets and the CWT is the one presented by Cartas-Rosado et al. [41], in which the ECG was sampled to analyze the heart rate variability and consequently estimated the automatic cardiac regulation. The CWT was used to extract the frequency bands of the ECG into three sub-bands labeled as high frequency, low frequency, and very low frequency. The parameterization of gamma was $\gamma = 3$, and the time-bandwidth product was set as $P^2 = 60$.

In a similar study, Byeon et al. [40] worked with the ECG signal for bio-metric identification performed by generating and scalogram of the ECG waveform through the Morse wavelet and selecting the default parameters of the MATLAB implementation. Additionally, Agarwal et al. [36] presented a subject-independent brain-computer interface by analyzing EEG data. This work aimed to measure imagined speech through EEG data and classify the EEG signals into four words (i.e., SOS, stop, medicine, wash-room) and one phrase (i.e., come-here) by employing a long-short-term memory. However, a comparison was performed with CNNs

by transforming the EEG into a scalogram using the Morse wavelet and feeding it to the CNN.

Furthermore, in the study of Smarr et al. [50], the CWT and the GMWs were used to analyze temperature data of patients with COVID-19 to identify patterns on the onset of fever. The gamma parameter was 3, and the beta parameter was set to 5. In previous studies presented by Smarr in [42], ultradian frequencies of core body temperature were studied through the CWT and used for the early detection and separation of pregnancy by employing a mouse model. Similarly, the parameters of the GMW were set as $\beta = 5$ and $\gamma = 3$. The WT has also been useful in the study of the epidemic evolution of COVID-19. For example, Campi et al. [48] analyzed the daily deaths per million caused by the COVID-19 epidemic and SARS-CoV-2 contagiousness measure through the RIC-index (i.e., the ratio of the time reproductive number and the doubling time). The Morse wavelet was used to generate the scalogram of the daily days data and RIC-index; however, the authors did not report the values of γ and β.

As presented in [50] time-frequency analysis tools have proven useful in analyzing patterns related to the onset of symptoms. Similar work was performed by Grant et al. [43] where the WT was used to analyze non-invasive measures associated with the reproduction system of women, such as the high-frequency distal body temperature, the sleeping heart rate, the sleeping heart rate variability, and the sleep timing to predict the preovulatory luteinizing hormone and provide a non-invasive method for fertility assessment. The WT analysis was performed using GMWs and establishing beta and gamma values to five and three, respectively.

Another common use of the WT is for filtering or denoising purposes. The above is crucial in physiological signal processing since the noise, or specific frequency bands, can alter the sampled signals, and their analysis [51]. For instance, the study of Wiklendt et al. [44] presented a technique that allows for the retention of frequencies that encode the periodicity of spike trains in EMG signals while filtering out frequencies that contribute to the morphologies of action potentials by employing the CWT. Similar to other studies presented in this study, the gamma parameter was set to 3, while the beta parameter was established as 1.58174. The value of β was determined heuristically.

Although it is widely used for time series data or 1D signals, the concept of the WT transform can be used for image and video processing. For example, in [52], the CWT was proposed to eliminate the distortions from remote PPG signal acquired from RGB videos to improve the estimation of non-contact pulse rate. Similar to other works, the gamma was set to 3 while the beta was selected based on the window length of the processed video. These window lengths were 32, 64, 128, and 256 frames. However, the authors did not report the exact values of the beta parameter for each window length.

Finally, the WT has also been implemented in closed-loop control strategies. The study of Davila et al. [49] sought to achieve a closed-loop modulation strategy of hippocampal oscillatory activity. The analysis was centered on hippocampal gamma power, a signal that has a known relationship with episodic memory processing. It is a potentially useful biomarker for manipulating memory performance. A linear quadratic integral servo controller is used to control the hippocampal gamma power. A wavelet filter bank performed through GMWs was employed to estimate the instantaneous root-mean-square gamma power. Gamma and the time-bandwidth product were equal to 3 and 60, respectively.

B. DYNAMICAL SYSTEMS ANALYSIS

GMWs have been used to study fluid dynamics, vibration analysis, and systems analysis. These topics can be associated with the field of dynamic systems analysis. This section presents a brief review of studies related to the abovementioned areas. Table 2 shows a summary of the studies and the parametrizations of the GMWs used in fluid dynamics, vibration analysis, and systems analysis. The parameters of the GMWs that are under parenthesis in Table 2 were estimated based on the expression shown in (13); nevertheless, they were not originally reported by the authors of the respective study.

1) FLUID DYNAMICS

The study of turbulent spots (i.e., concentrations of vortices with high eddy strength) has been carried out using GMWs. For example, Wang et al. [57] study the early emergence of artificially induced turbulence patches across a flat plate in a laminar boundary layer in a low-turbulence wind tunnel. The GMWs were used to analyze the downstream variation in the turbulence energy distribution within incipient turbulent spots. Similarly to other works that have used the GMWs, gamma and time-bandwidth product were set to 3 and 60, respectively. Besides, in a recent investigation of the authors mentioned above presented in [58], GMWs were used to study the downstream variation in the turbulence energy distribution within incipient turbulent spots. The set of parameters of the GMWs remains the same. However, the study focused on applying opposition control of artificially initiated turbulent spots.

On the other hand, Riches et al. [53] utilized proper orthogonal decomposition (POD) to study the wake-dynamics of a low-mass ratio circular cylinder that is experiencing upper and initial branch vortex-induced vibrations. In particular, the CWT and GWWs were employed to generate a time-frequency representation that clarifies how different POD mode pairs interact. This study tested different beta and gamma values; nevertheless, the authors reported that the results were insensitive to different values of the time-bandwidth product parameter. The final setting of the GMWs parameters were $\beta = 120$ and $\gamma = 3$. Otherwise, Liu et al. [54] studied the temporal and spatial evolution of sand ripples and waves in a turbulent boundary layer airflow. The CWT and the GMWs were used to analyze the time series of the sand bed height fluctuations in separate streamwise positions. Yates et al. [55] used the CWT and the Morse wavelets to determine the spatial wavenumber distributions

TABLE 2. Summary of the parametrizations used for Generalized Morse Wavelets in fluid dynamics, vibration analysis, and systems analysis.

Author	Year	Parameters of GMWs	Analyzed signal, system, or process	Application of the GMW
Fluid Dynamics				
Riches et al. [53]	2018	$\gamma = 3, \beta = 120$ ($P^2 = 360$)	Interaction of proper orthogonal decomposition mode pairs	Analysis of the wake dynamics of a low-mass ratio circular cylinder under branch vortex-induced vibrations.
Liu et al. [54]	2020	Not reported	Time series of the sand bed height fluctuations	Analysis of the temporal and spatial evolution of sand ripples and waves in a turbulent boundary layer airflow.
Yates et al. [55]	2020	$\gamma = 3, P^2 = 60$ ($\beta = 20$)	Heat-flux profiles	Determination of the spatial wavenumber distributions of stationary cross-flow waves.
Lelong et al. [56]	2020	Not reported	Wave signal	Analysis of strong near-inertial wave signals at the base of the semipermanent anticyclonic Cyprus Eddy.
Wang et al. [57]	2021	$\gamma = 3, P^2 = 60$ ($\beta = 20$)	Analysis of the downstream variation in the turbulence energy distribution	Study the early emergence of artificially induced turbulence patches across a flat plate in a laminar boundary layer in a low-turbulence wind tunnel.
Wang et al. [58]	2022	$\gamma = 3, P^2 = 60$ ($\beta = 20$)	Analysis of the downstream variation in the turbulence energy distribution	Application of opposition control of artificially initiated turbulent spots.
Vibration Analysis				
Abuhamdia et al. [59]	2018	$\gamma = 3, P^2 = 60$ ($\beta = 20$)	Mechanical vibrations	Decoupling modes of mechanical vibrations.
Baldini et al. [60]	2020	Not reported	Vibration signal	Classification of road surface anomalies through CNNs.
Khan et al. [61]	2021	$\gamma = 3, P^2 = 60$ ($\beta = 20$)	Vibration signal	Fault diagnosis of a shaft-disk system through the CWT and CNNs.
Garro et al. [62]	2021	Not reported	Vibroacoustic response of latch door	Analysis of the automotive door latch acoustic response when closing.
Civera et al. [63]	2022	$\gamma = 3, \beta = 20$ ($P^2 = 60$)	Gearbox vibrations of wind turbines	Estimation of the instantaneous spectral entropy for fault diagnosis in wind turbines.
Civera et al. [64]	2022	$\gamma = 3, \beta = 20$ ($P^2 = 60$)	Vibration signal	Detection of sudden damage-related to structural changes of civil structures and infrastructures.
Systems Analysis				
Mahato et al. [65]	2019	Not reported	Three degree of freedom hypothetical system, Building under earthquake excitation, Thin beam with lumped masses	Model parameter identification through the synchrosqueezed wavelet transform.
Jin et al. [66]	2019	Not reported	Non-linear assemble structures system identification	Non-linear system identification performed through Morse wavelets.
Wang et al. [67]	2020	$\gamma = 3, \beta = 27$ ($P^2 = 81$)	Civil structures	Identification of structural time-varying parameters for structural health monitoring.
Magriri et al. []	2020	$\gamma = 3, \beta = 20$ ($P^2 = 60$)	Time series of iron electrodissolution	Approximation of slow and fast dynamics from time series that is characterized by local scales in the time domain.
Yan et al. [68]	2020	Not reported	Dynamic Reproduction of Projectiles in Ballistic Environments for Advanced Research testbed	Real-time state estimation for high-rate systems.
Zhu et al. [69]	2021	$\gamma = 3, \beta = 3.1$ ($P^2 = 9.3$)	Bridge weight-in-motion system	Monitoring of the vehicle bridge weight-in-motion system through the CWT and CNNs.
Mitra et al. [70]	2022	$\gamma = 3, P^2 = 60$ ($\beta = 20$)	Control of a wind turbine tower	Frequency-dependent gain scheduling for optimal tuning based on the WT.
Lanning et al. [71]	2022	$\gamma = 3, P^2 = 60$ ($\beta = 20$)	Nonlinear structural systems	Calibration of parameters of structural systems through CWT and CNNs.

of stationary cross-flow waves from experimental data. The parameters of the Morse wavelet, similar to other studies presented, were 3 for the value of gamma and 60 for the time-bandwidth product.

Finally, Lelong et al. [56] investigated how near-inertial/eddy interactions affect energy removal from the mixed layer by analyzing observations from strong near-inertial wave signals at the base of the semipermanent anticyclonic Cyprus Eddy. A hybrid temporal-spatial decomposition was proposed to study the flow dynamics of the eddy. The CWT and the GMWs were used to analyze the wave signal. However, the parametrization of the Morse wavelet was not reported in the study.

2) VIBRATION ANALYSIS

Mechanical vibration analysis performed through time-frequency analysis methods has also been carried out with the help of GMWs. An instance of this was reported by Abuhamdia et al. [59]; this study introduced the theory of the so-called Laplace Wavelet Transform to analyze the decoupling modes of mechanical vibrations; the results were compared with the results obtained through the GMWs. Like other studies mentioned in this review, gamma was established as 3, while the time-bandwidth product was set at 60. Moreover, the classification of vibration signals for road surface assessment applied through GMWs was proposed by Baldini et al. [60]. The previous study compared the spectrogram of the STFT and the scalogram of the WT generated by a Morse wavelet to classify road surface anomalies through the processing of accelerometer signals. Nevertheless, the authors did not report the setting of the Morse wavelet parameters. In [61], fault diagnosis of a shaft-disk system was performed through transfer learning and pre-trained CNNs. The input to this CNN model was the scalogram of the vibration signal sensed in the rotor system. The time-frequency representation was generated via the GMWs by utilizing the default values of its parameters of the MATLAB implementation.

Vibroacoustic responses have also been studied using the WT and GMWs. For example, Garro et al. [62] studied the primary influence of an automotive door latch's acoustic response when closing. Three door latch components' transient sound pressure level responses were collected and analyzed. The spectral decomposition of the acoustic response was investigated using the CWT, but the authors did not disclose the Morse wavelet parameters. Finally, Civera et al. [64] proposed to employ the instantaneous spectral entropy and CWT to analyze the gearbox vibrations of wind turbines for anomaly detection and defect diagnostics. This is one of the few studies in which an extensive explanation and analysis of different values of gamma and beta were presented while establishing the parameters to compute the CWT and performing a sensitivity analysis of the instantaneous spectral entropy estimation. The above led the authors to conclude that the optimal values of gamma and beta for this particular application were $\gamma = 3$ and $\beta = 20$. The authors used the same values of beta and gamma in [63] to estimate the instantaneous spectral entropy of vibration signals for detecting sudden damage related to structural changes of civil structures and infrastructures.

3) SYSTEMS ANALYSIS

As mentioned in the previous sections, the CWT and the GMWs have been used to analyze fluids and vibrations. This section presents a summary of the application of this wavelet function for analyzing dynamical systems. Magrini et al. [72] presented a methodology based on the CWT for approximating slow and fast dynamics from time series characterized by local scales in the time domain. In this study, the values of gamma and beta of the GMWs were chosen to be 3 and 20, respectively. The methodology was tested on a time series of iron electrodissolution characterized by slow chaotic dynamics and irregular spiking. Parameter identification of time-varying systems has been performed with the help of the WT. In [67], it was proposed to identify the structural time-varying parameters with the combination of variational mode decomposition and GMWs for structural health monitoring. The parameters γ and β were set as 3 and 27, respectively.

Similarly, Lanning et al. [71] examine the use of machine learning to calibrate the parameters of analytical models of nonlinear structural systems due to the lack of data in this area. The chosen machine learning architecture were CNNs, whose inputs were scalograms obtained through the CWT and GMWs. Similar to other works presented in this review, the values of the gamma and the time-bandwidth product were 3 and 60, respectively.

Another example of parameter identification is shown by Mahato et al. [65], where the synchrosqueezed WT was proposed for this purpose. The GMWs were selected to compute the synchrosqueezed WT. The method was tested on different systems, such as a three-degree-of-freedom hypothetical system, a building under earthquake excitation, and a thin beam with lumped masses. Furthermore, employing time-frequency representations and wavelets has also approached nonlinear system identification. For example, Jin et al. [66] proposed to identify assembled nonlinear structures systems by comparing the STFT, Hilbert transform, zero-crossing, restoring force surface, restoring force, neural networks, and Morse wavelets.

As can be appreciated from the previous studies, the analysis of structural systems has been performed through GMWs. Another example of this is shown in [73], where a wireless large-area strain sensor (WLASS) was used to measure large-area strain fatigue cracks of steel bridge structures under traffic loading. The CWT was used to analyze the WLASS data by setting the parameters of GMWs as follows $\gamma = 1.5$, and $P^2 = 3$.

Moreover, GMWs have also been utilized for control engineering strategies. For example, Mitra et al. [70] presented a control strategy based on the WT for a wind turbine tower with an onshore horizontal axis vibration. The WT is used to perform a frequency-dependent gain scheduling for optimal tuning. Besides, the WT was used to transform the

controller's input and feedback to remodel a linear quadratic regulator in the time-frequency domain. The authors of this study employed the default values of the parameters of the GMWs available in MATLAB.

Automatic vehicle system monitoring methods have also been conceived through the CWT. For example, Zhu et al. [69] provided a procedure for vehicle monitoring of a bridge weigh-in-motion system based on acceleration and employing deep learning and the WT. The CWT was used to generate scalograms to train a CNN for detecting a valid sequence from the acceleration data and for valid axle localization performed with an adaptive wavelet method. The mother wavelet used to develop this system was a GMWs with $\gamma = 3$ and $\beta = 3.1$. Finally, Yan et al. [68] compare time-frequency methods such as the WT, the STFT, WVD, synchrosqueezed transform, and multi-synchrosqueezed transform to perform real-time state estimation for high-rate systems. In particular, the authors selected the Morse wavelet to compute the WT. The study used the experimental data from the Dynamic Reproduction of Projectiles in Ballistic Environments for Advanced Research testbed [74].

C. ELECTRICAL ENGINEERING

The analysis of electrical power systems refers to the network of electrical devices constructed to provide, transmit, and use electrical energy. This section presents the application of the GMWs and the CWT related to electrical power systems and electrical engineering. Table 3 shows a summary of the investigations and the parametrizations of the GMWs used in electrical engineering. The parameters of the GMWs under parenthesis in Table 3 were estimated based on the expression shown in (13). Nevertheless, they were not initially conveyed by the authors of the respective study.

In this context, Allan et al. [76] proposed an islanding detection method for renewable-based distributed energy resources. The proposed algorithm was based on a CNN that used as input the scalogram of the voltage islanding signal generated with the help of GMWs. Besides, Seyedi et al. [77] studied the post-fault transient response in hybrid AC/DC microgrids by performing a time-frequency decomposition using the CWT. The CWT was applied to data from simulations of electromagnetic transients in grid-connected and islanded modes of operation. The Morse wavelet was parametrized with gamma equal to 3 and a time-bandwidth product of 120. Furthermore, Abedini-Livari et al. [75] used phase-resolved partial discharge patterns to examine the effects of contaminated layer and housing-erosion on partial discharges at the insulator surface. The CWT and GMWs were used on the partial discharge signals to identify polluted insulators used on power grids.

The condition of elements used in power systems has also been studied with GMWs. For instance, in [78], the health of a dc-link capacitor inside a three-phase inverter was monitored through the CWT and machine learning. The CWT was used to analyze the conducted electromagnetic interference, and the classification was performed with a support vector machine. Similar to other research works presented in this study, the parameters of the Morse wavelet were established as follows, the gamma parameter was equal to 3, the time-bandwidth product was 60, and the voices or wavelets per octave were established to be 10. Fault diagnosis of induction motors has also been studied with the help of Morse wavelets and the CWT. For instance, Pasqualotto et al. [11] employed the CWT on the signal of the stator current during the startup of an induction motor to generate a scalogram that could be used as input to a 2D CNN to detect faults related to broken bars in induction motors. The authors did not detail the parameters of the GMWs. However, the analyzed frequency range was reported to be from 5 to 60 Hz, and the decomposition level of the CWT was 36.

The analysis of power sources, such as battery state health, has also been studied through the CWT and GMWs. For example, Nusev et al. [12] used a discrete random binary sequence-based broadband electrochemical impedance spectroscopy to measure changes in the battery input to make less intrusive the operation process of the battery and monitor its condition. The impedance was analyzed by processing current and voltage signals through the CWT and GMWs. The value of gamma and beta were not mentioned in this study.

D. GEOPHYSICS

As mentioned in Section III. The WT concept was first introduced in the geophysics field by Morlet et al. [5] in the early 1980s. More recently, GMWs have also been used to analyze seismic data. This section presents a brief review of research that has employed this wavelet family for geophysics analysis. Table 4 shows a summary of the studies and the parametrizations of the GMWs used in geophysics. The parameters of the GMWs under parenthesis in Table 4 were estimated based on the expression shown in (13); nevertheless, they were not originally reported by the authors of the respective study.

Wang et al. [79] presented an approach to estimate the instantaneous frequency of seismic data through the wavelet domain. The approach was compared with the instantaneous frequency results obtained through the Hilbert transform. According to the authors, the proposed method based on the GMWs and the WT showed a higher precision and anti-noise performance than the Hilbert transform. The setting of γ and β was set to 3 and 1, respectively. In [80], the same values for γ and β were used to perform a spectral decomposition of 3D seismic data to detect fluvial channels with thickness around. The above parametrization of GMWs was also compared with the Morlet wavelet, where the GMWs demonstrated better performance for time localization than the Morlet wavelet.

Witney et al. [81] examined GMWs to determine their capacity to derive ground motion pulses from a collection of acceleration samples. Different sets of values P and γ were tested. From the presented analysis, gamma was set equal to 2 and the inverse bandwidth (P) equal to 4. Wang et al. [82] worked with the GMWs to develop a machine-based

TABLE 3. Summary of the parametrizations used for Generalized Morse Wavelets in electrical engineering applications.

Author	Year	Parameters of GMWs	Analyzed signal, system, or process	Application
Abedini-Livari et al. [75]	2020	Not reported	Partial discharge signals	Identification of contaminated insulators used on power grids.
Allan et al. [76]	2021	Not reported	Voltage islanding signal	Islanding detection for renewable-based distributed energy resources performed through the CWT and CNNs.
Seyedi et al. [77]	2021	$\gamma = 3$, $P^2 = 120$ ($\beta = 40$)	Electromagnetic transients in grid-connected and islanded modes of operation	Study of the post-fault transient response in hybrid AC/DC microgrids through the CWT.
Pasqualotto et al. [11]	2021	Not reported	Stator current signal of induction motor	Detection of faults related to broken bars in induction motors.
Nusev et al. [12]	2021	Not reported	Impedance analysis through current and voltage signals	Health monitoring of batteries.
Mcgrew et al. [78]	2022	$\gamma = 3$, $P^2 = 60$ ($\beta = 20$)	Electromagnetic interference of three-phase inverters	Monitoring the health of a DC-link capacitor.

TABLE 4. Summary of the parametrizations used for Generalized Morse Wavelets in geophysics.

Author	Year	Parameters of GMWs	Analyzed signal, system, or process	Application
Wang et al. [79]	2013	$\gamma = 3$, $\beta = 1$ ($P^2 = 3$)	Seismic data	Estimation of instantaneous frequency from seismic data performed through the CWT.
Wang et al. [80]	2016	$\gamma = 3$, $\beta = 1$ ($P^2 = 3$)	3D Seismic data	Detection of fluvial channels with thickness around through the CWT.
Whitney et al. [81]	2019	$\gamma = 2$ $P = 4$	Acceleration seismic data	Derivation of ground motion pulses.
Wang et al. [82]	2020	$\gamma = 3$, $\beta = 1$ ($P^2 = 3$)	Seismic data	Determination of the Sulige gas field's tight-sand reservoir's thickness.
Lurka et al. [83]	2021	Not reported	Seismic data	Characterization of the time-frequency properties of the ground motions produced by seismic sources.
Moriya et al. [84]	2021	$\gamma = 3$, $P^2 = 60$ ($\beta = 20$)	Acoustic emission waveform	Determine the relative source location of seismic events.
Yuan et al. [85]	2021	Not reported	Ground motion time series	Image encoding of ground motion time series performed through the CWT.

system for seismic spectral attribute analysis to determine the thickness of the Sulige gas field's tight-sand reservoir. The parameters of the Morse wavelets were selected based on a three-layer wedge model whose rock parameters are from a tight reservoir. The above led to choosing a value of beta equal to 1 and gamma equal to 3. Furthermore, Lurka et al. [83] employed the CWT and Morse wavelets to characterize the time-frequency properties of the ground motions produced by seismic sources in underground mines. Nonetheless, the values of gamma and beta were not reported.

As can be appreciated, seismic data evaluation performed through the WT is particularly interesting in the literature. Moriya et al. [84] used the GMWs and the CWT to calculate the phase-only correlation function to find similar acoustic emission waveforms. These waveforms must be detected to determine the relative source location of seismic events. The detection of acoustic emission is crucial since acoustic emission provides information on fracture systems, like the orientation of fractures in geothermal reservoirs. The setting of the GMWs was $P^2 = 60$ and $\gamma = 3$.

Finally, Yuan et al. [85] proposed an image encoding technique performed through time series segmentation that transforms acceleration, velocity, and displacement ground motion time series into a three-channel image of the ground motion. This image is used as input for a CNN for seismic damage evaluation. The proposed encoding technique was compared with traditional methods, such as the CWT computed through Morse wavelets.

E. COMMUNICATIONS SYSTEMS

The processing and analysis of information employed in communications systems have also been performed through GMWs. Examples of its applications are described in this section. Table 5 shows a summary of the studies along with

TABLE 5. Summary of the parametrizations used for Generalized Morse Wavelets in communication systems.

Author	Year	Parameters of GMWs	Analyzed signal, system, or process	Application
Tahir et al. [86]	2019	Not reported	Wireless Channel State Information	Classification of the freezing of gait of Parkinson disease patients through the CWT and CNNs.
Ujan et al. [87]	2020	Not reported	Digital video streams as signal of interest	Detection and characterization of radio frequency interference in wireless communications networks.
Ssekidde et al. [88]	2021	Not reported	WiFi received signal strength indicators data	Indoor localization performed through the CWT and CNNs.
Niu et al. [89]	2022	$P^2 = 120$ Gamma value was not reported.	Doppler's frequency shift in WiFi-based contactless sensing systems	Velocity estimation through WiFi sensor systems.
Kim et al. [90]	2022	$\gamma = 3, \beta = 40$ $(P^2 = 120)$	Radar based system	Human activity recognition by employing the CWT and CNNs.
Walenczykowska et al. [91]	2022	$\gamma = 27, \beta = 27$ $(P^2 = 729)$	Radar waveforms	CWT is used for feature extraction and radar signal recognition.

the parametrizations of the GMWs used in communication systems. The parameters of the GMWs under parenthesis in Table 5 were estimated based on the expression shown in (13); nevertheless, they were not reported by the authors of the respective study.

The study presented by Tahir et al. [86] proposed to classify the freezing of gait (i.e., episodic absence of forward movement) of patients who have Parkinson's disease by analyzing the ambient 5G spectrum and processing the amplitude changes of the wireless Channel State Information (CSI). The CSI signal was processed with the help of the CWT and GMWs to produce a scalogram of the 1D signal, which was input into a CNN model for freezing of gait detection. Nonetheless, the parameters of the Morse wavelet were not reported by the authors.

In addition, Ssekidde et al. [88] tested the GMWs and CWT to process and extract features from WiFi-received signal strength indicators data to develop an algorithm for indoor localization. The proposed CWT-based features were tested with a CNN and compared with an artificial neural network. In addition, a comparison with the features extracted by computing the CWT with the Morlet wavelet was performed. Similar to Tahir's study, the authors did not specify the parameters of the GMW. Similarly, Niu et al. [89] examine how target locations and headings affect the velocity estimation accuracy in WiFi-based sensor systems. The CWT and the GMWs were used to determine the Doppler frequency shift that is associated with the target velocity in WiFi-based contactless sensing systems. The time-bandwidth product of the GMWs was defined to be 120, the gamma parameter was not reported, and the number of voices or wavelets per octave was set to 10.

Furthermore, Ujan et al. [87] employed the transfer learning framework to detect and characterize radio frequency interference in wireless communications networks [92]. The objective was to identify the signal nature and modulation type of received signals. The CWT was applied through GMWs on the received signals by considering digital video streams as a signal of interest. The parameters of the Morse wavelet were not mentioned in the study above. Likewise, Kim et al. [90] presented a radar-based system for human activity recognition by employing the CWT and GMWs. The parameterization of the Morse wavelet was $\beta = 40$ and $\gamma = 3$. The CWT was used to generate range-time-Doppler maps to train a CNN to classify human activities such as walking, falling, sitting, standing up, picking an object from the floor, and drinking water.

Finally, Walenczykowska et al. [91] proposed an algorithm for radar signal recognition. The classified radar waveforms included the near frequency modulated pulsed waveform, the stepped frequency modulated pulsed waveform, the phase coded pulsed waveform, frequency modulated continuous wave, and the Phase Coded Continuous Waveform to provide a potential use for Electronic Warfare. The data was processed with the help of the CWT applied through the GMWs and higher-order statistics for feature extraction. The classification was performed with the use of an artificial neural network. A throughout analysis was performed to determine the appropriate values of the parameters of GMWs, which led to select $\gamma = 27$, and $\beta = 27$.

V. DISCUSSION

As presented in the previous sections, GMWs have proven helpful in analyzing diverse signals, systems, and processes, including fields that go from medical or biomedical engineering to geophysics. The above sustain the claim of Lilly et al. [18] related to the potential of GMWs for general-purpose use. In addition, most of the reviewed literature using the CWT and the GMWs pertains to biomedical or medical fields. The above suggests the widespread acceptance of the WT in

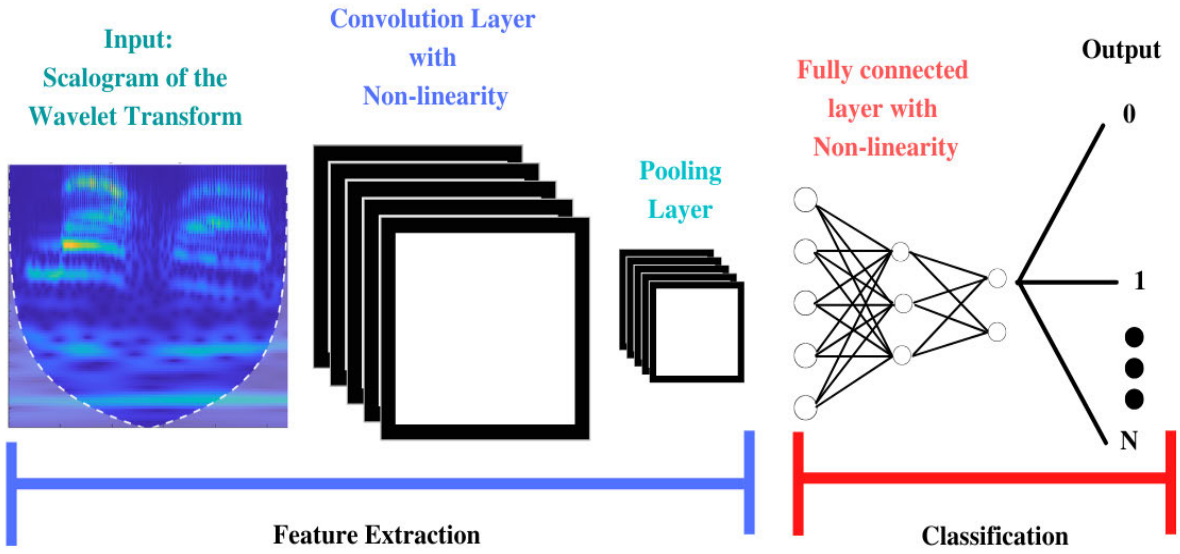

FIGURE 5. General architecture of a Convolutions Neural Network trained with the scalogram generated through the Continuous Wavelet Transform and Generalized Morse Wavelets employed for detection and classification tasks. The scalogram is incorporated in the feature extraction stage of the algorithm, serving as an image of the original 1D signal. The feature extraction is performed through the convolution and pooling layers, while the classification is generally performed with a fully connected layer. The output can have *N* classes depending on the characteristics of the classification problem.

biomedical or medical systems analysis. Other areas in which the WT has been used extensively are analyzing complex dynamical systems such as fluid dynamics, mechanical vibrations, systems identification, and control engineering strategies. Furthermore, electrical engineering, geophysics, and communication systems are other areas that have employed the Morse wavelet family.

The reviewed literature shows that a typical use of GMWs is to employ the obtained scalogram produced by these wavelets to perform classification tasks by employing machine learning algorithms. Mainly, the algorithm that is preferred are CNNs. The above is supported by the studies presented in Section IV. The general structure of this methodology is shown in Fig. 5. The scalogram of the CWT is used as input for CNNs and performs the feature extraction on this 2D image of the original 1D time series through the convolution, and pooling layers [93]. The classification is generally performed through a fully connected layer. Thus, there is a trend in the overall literature to take advantage of the time-frequency localization provided by the CWT and GMWs of 1D signals or time series data and use it as input to deep learning architectures to solve classification problems, mainly through CNNs.

Furthermore, it is essential to remark that most of the classification tasks performed through the use of the WT are biomedical signals and communication systems. To a lesser extent, other areas, such as vibration analysis, and electrical engineering, as presented in Tables 2, 3, and 5 have performed classification through the GMWs. Although the WT can be coupled with CNNs to perform detection and classification tasks, one of the main drawbacks of this methodology is the high computational power required to perform the CWT, and the training of the CNNs [94]. Furthermore, the CWT transform may require a high memory capacity since this technique generates many coefficients. The redundancy could be mitigated with the dyadic sampling strategy of the discrete wavelet transform but applied through GMWs.

Another challenge of this approximation is that even though the CWT and GMWs can provide a 2D representation of the 1D signal that could be used as input to the CNN, the setting of an adequate architecture of this CNN could be challenging, as reported by Pasqualotto et al. [11]. One possible solution to this task is to used pretrained CNNs such as GoogleNet [95], AlexNet [96], ResNets [97], or DenseNets [98], and apply the transfer learning framework to fine-tune the architectures mentioned above. Another potential advantage of transfer learning is that it does not require a large sample size to perform the training procedure [99]. For example, transfer learning applied through CNNs plus GMWs has been used by Ujan et al. [87] for detecting radio frequency interference in wireless communication networks and by Khan et al. [61] for fault diagnosis of a shaft-disk system. Nonetheless, if interpretability is sought for the classification algorithms, CNNs may not be appropriate due to their black box structure [100].

In addition, most of the studies that employed the GMWs used the MATLAB implementation to perform their analysis or the package provided by Lilly et al. [29]. One of the drawbacks of the MATLAB implementation is the need for a license, which can be unaffordable for research centers, universities, and authors to perform their research. Nevertheless, the MATLAB implementation has extensive documentation, implementation examples, and a support community. On the other hand, the jLab package provided by Lilly et al. [29] has reduced documentation and examples compared to MATLAB. The above suggests the opportunity to implement this wavelet family and, consequently, the WT in other software platforms such as R, Octave, or Julia. In addition, it will be essential to generate a well-documented implementation in the software mentioned above that help to perform reproducible results within areas or applications. Recently, Chu et al. [101] presented GhostiPy, a package for Python that implements the GMWs; however, due to its recent publication, this package has yet to be widely used to assess the quality of the implementation.

One of the major drawbacks in the reviewed literature is that certain studies that have used GMWs should have reported the values of both gamma and beta that were selected to perform the CWT analysis. The above was also depicted in Tables 1, 2, 3, 4, and 5. This lack of reported information in the studies introduces a problem of reproducibility in the current literature. Besides, another crucial piece of information that is often overlooked while computing the CWT through Morse wavelets is the number of filters per octave or the size of the filter bank that the authors used to develop their analysis or applications. These parameters could comprise the expected results since they need to be determined based on the characteristics of the systems, signal, or process being investigated. The above was also pointed out by Civera et al. [64] while performing instantaneous spectral entropy estimations using the GMWs.

On the other hand, concerning the articles that have reported the values of gamma and beta. Regardless of its applications, most authors have used the default parametrization set in MATLAB for GMWs, and the CWT. In those cases, gamma was set to 3, and the time-bandwidth product was set to 60. On the one hand, this suggests a typical value that could be used for time-frequency analysis carried out using the CWT for a diverse set of fields or applications, as depicted in Section IV. On the other hand, it suggests the lack of a robust argumentation and justification considered by the authors to explain why a specific value of gamma or beta was selected. The above could be critical for adequately representing a function's spectro-temporal content. Thus, further investigation could be performed to determine an appropriate or optimal value of gamma, beta, or the time-bandwidth product for the applications reviewed in this study. Possible proposals could explore the use of optimization algorithms to determine the suitable values of gamma and beta or to carry out trial and error tests and analyze the obtained scalogram under different values of gamma and beta [102].

Another aspect to remark on is that even among equal signal types analyzed through the GMWs, different parameterizations have been considered. For instance, Wachowiak et al. [37] set gamma equal to 3 and beta equal to 4 for analyzing ECG signals, while on the other hand, Byeon et al. [40], and Cartas-Rosado et al. [41] employed gamma equal to 3 and beta equal to 20 for ECG signals. This difference in beta values could be related to the information the authors intended to extract from the ECG signal through the WT or the application they developed in their respective research. Nonetheless, as explained previously, there needs to be a deeper argumentation and discussion when selecting the parameters of Morse wavelets.

As explained in the study of Tian et al. [103], an adequate wavelet selection can influence the obtained results while analyzing seismic data. Likewise, Walenczykowska et al. [91] also studied the effects of Morse wavelet parameters when analyzing radar waveforms. On the other hand, Riches et al. [53] mentioned that the analysis of POD pairs performed through the CWT and GMWs was insensitive to the values of the time-bandwidth product. These studies highlight the importance of adapting the values of gamma and beta based on the type of signals or systems under investigation. Since, in some applications, these values may influence the results. Nevertheless, the effects of the Morse wavelet's different parametrizations for particular applications are yet to be performed extensively.

On the other hand, by analyzing the reported values of gamma and beta, it could be possible to study only the effect of the beta parameter on the obtained scalogram since most of the referred studies selected a value of $\gamma = 3$. According to Lilly et al. [18] and as explained in Section III when $\gamma = 3$ the GMWs get near the lower-bound of the Heisenberg area (i.e., $A_\psi = 0.5$). Thus, taking the values of the Heisenberg area as a reference to fix the value of gamma to approximate the Heisenberg area lower-bound, the analysis of the effect of the beta parameter on the scalogram and time-frequency resolution that is obtained can be studied with further detail. Nevertheless, it is essential to remark that there are other regions in the parameters space of the GMWs aside from $\gamma = 3$ that get close to this Heisenberg area lower-bound as illustrated in Fig. 4. Thus, there is an opportunity to explore the behavior of the GMWs in other regions of their parameter space.

Otherwise, the GMWs' frequency resolution increases when the beta value becomes bigger since the bandpass filter becomes narrower (see Fig. 3). However, on the other hand, the time resolution of the wavelet functions decreases. Therefore, the effect of fixing gamma and increasing the beta value can be understood in terms of the changes in the standard deviation of the wavelet function in the time and frequency domains.

The above is illustrated in Fig 6. Fig. 6a shows the behavior of the time domain standard deviation of the GMWs for increasing values of β and $\gamma = 3$. Fig. 6b shows the behavior of the frequency domain standard deviation of the GMWs

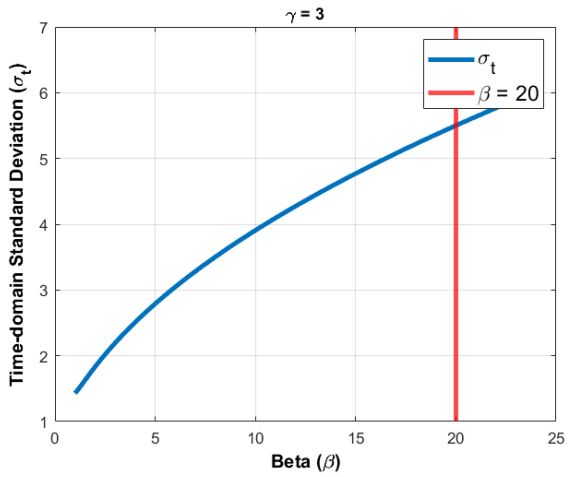

(a) Time domain standard deviation

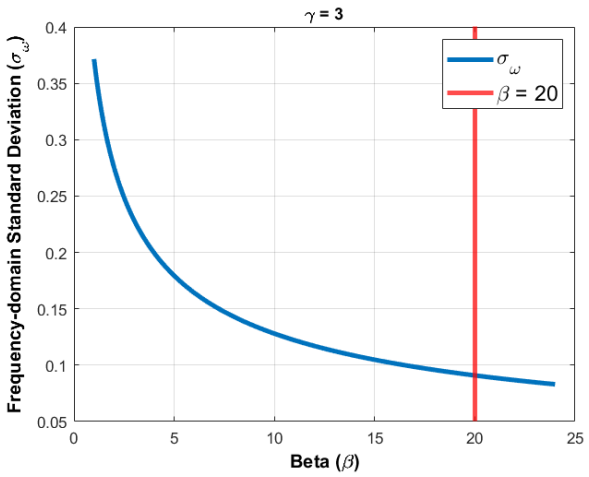

(b) Frequency domain standard deviation

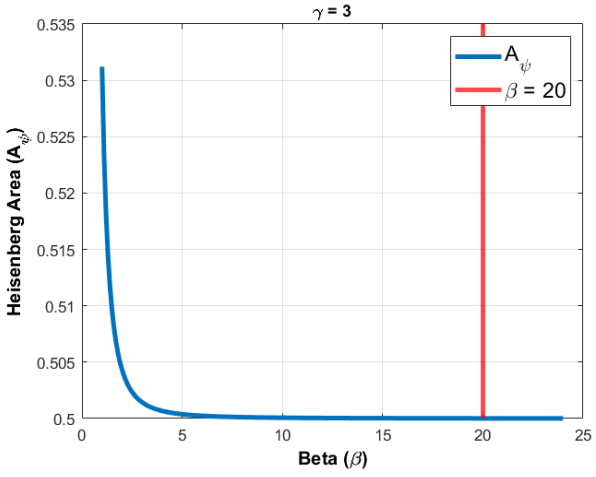

(c) Heisenberg area

FIGURE 6. The behavior of the standard deviation of the Generalized Morse Wavelets in the time and frequency domains and Heisenberg area for increasing values of beta and a constant gamma with a fix value of three. a) Shows the behavior of the standard deviation in the time domain of the Generalized Morse Wavelets for increasing values of beta depicted by the blue line; the vertical red line denotes the value of beta equal to 20, a typical selection employed in the literature along with gamma equal to 3. b) Shows the behavior of the standard deviation in the frequency domain of the Generalized Morse Wavelets for increasing values of beta depicted by the blue line; the vertical red line denotes the value of beta equal to 20, a typical selection employed in the literature along with gamma equal to 3. c) Shows the behavior of the Heisenberg area of the Generalized Morse Wavelets for increasing values of beta displayed in blue. The vertical red line denotes the beta value equal to 20, a typical selection of beta used in the literature in combination with gamma equal to 3.

for increasing values of β and $\gamma = 3$. Finally, Fig. 6c illustrates the behavior of the Heisenberg area for increasing values of β and $\gamma = 3$. Notice that by growing the beta value, the standard deviation in the time domain increases, which impacts the time localization of the wavelet function. Otherwise, the standard deviation of the frequency domain function decreases. By comparing Fig. 6a and 6b, the magnitude of the standard deviations had a notable difference in their magnitudes, with the values of the standard deviation of the frequency domain function being lower than 0.4, and the standard deviation of the time domain function is greater than 1. The above implies that most of the applications that have used the GMWs by considering $\gamma = 3$ have better frequency resolution but at the cost of having a lower resolution in time.

For the sake of completeness and to complement the information presented in Fig. 6, the specific values of the standard deviation of the time and frequency domain of GMWs are presented in Table 6. In addition, the Heisenberg area for the values of gamma and beta used in the literature are presented in the same Table. Notice that for values of β greater than five, the Heisenberg area is practically equal to 0.5; nonetheless, in this part of the whole parameter space of the GMWs the spread in the time domain is greater than in the frequency domain as discussed earlier.

The vertical red line presented in Fig. 6 indicates the value of $\beta = 20$. This value is a common choice in the literature for using the GMWs, along with $\gamma = 3$, as presented in Section IV. This setting of gamma and beta leads to a time-bandwidth product of $P^2 = 60$ based on the expression shown

TABLE 6. Values of the standard deviation in the time and frequency domains and Heisenberg area of the Generalized Morse Wavelets for the shared values of its parameters used in the reviewed literature.

Gamma (γ)	Beta (β)	Time-Bandwidth Product (P^2)	Time domain Standard Deviation (σ_t)	Frequency domain Standard Deviation (σ_ω)	Heisenberg Area (A_ψ)
2	8	16	2.8752	0.1754	0.5044
3	1.58174	4.74522	1.6629	0.3056	0.5083
3	1	3	1.4298	0.3715	0.5312
3	3.1	9.3	2.2275	0.2251	0.5013
3	4	12	2.5093	0.1995	0.5007
3	5	15	2.7904	0.1793	0.5004
3	8	24	3.5031	0.1428	0.5001
3	20	60	5.5008	0.0909	0.5000
3	40	120	7.7624	0.0644	0.5000
3	27	81	6.3841	0.07843	0.5000
3	120	360	13.4258	0.0372	0.5000
27	27	729	19.1114	0.0288	0.5510

in (15). As discussed earlier, this is the default parametrization available in the MATLAB implementation of the CWT and GMWs. This parametrization shows a standard deviation in the time domain of 5.5008 and of 0.0909 in the frequency domain. Furthermore, its Heisenberg area is close to one-half, as shown in Table 6. Thus, this implies that the studies that have chosen the default parametrization of the MATLAB implementation of GMWs have a lower time resolution and a greater frequency solution when computing the CWT. Nevertheless, the authors did not present an analysis that expands on the implications of the time-frequency representation obtained through this parametrization of GMWs for the investigated signals, systems, or processes.

Finally, another parameter often overlooked when the use of the CWT and GMWs is reported is the size of the filter bank or the number of voices per octave the authors decided to employ to perform the CWT. This parameter influences the frequency resolution obtained when computing the CWT since it allows controlling the discretization of the scales of the CWT [104]. A higher value of voices per octave implies a better scale resolution; however, the number of computations increases. On the other hand, a lower number of voices per octave is related to a lower scale resolution and a lower number of computations. Despite the importance of the voices per octave in the scales resolution and the computations involved in performing the CWT, a profound analysis of its selection, implications, and interaction with the gamma and beta parameters of GMWs has not been studied extensively.

VI. LIMITATIONS OF THE STUDY

This paper was mainly focused on the applications of the GMWs and, consequently, the CWT. Thus, other wavelet transformations were not considered since the GMWs are mainly used with the CWT rather than the discrete wavelet transform, fractional wavelet transform, synchrosqueezed WT, wavelet packet decomposition, or TQWT [16]. One exception is the study of [65], where the synchrosqueezed WT was computed with GMWs. However, the above implies that there could be better options than the use of the GMWs for analyzing the referred applications and that other wavelet families or time-frequency representations could be more efficient or effective in performing specific analyses or uses. For instance, if the computational cost and sparsity are crucial criteria to develop the study, the discrete wavelet transform, and orthogonal wavelets could be better options for compression tasks than the CWT and the GWMs. In addition, as mentioned earlier, using the CWT in these studies could outperform other time-frequency analysis techniques like the HHT or even the STFT. Nevertheless, studies that conduct these comparisons or analyses could be further developed or searched within the existing literature.

Another limitation of the present study is the fields that were reviewed. As presented previously, this literature review organized the articles in the following areas: medical and biomedical engineering, dynamical systems analysis, electrical engineering, geophysics, and communications systems. Nevertheless, there are other fields in which the GMWs have also been used, such as physiology [105], image processing [106], and signal processing theory [107], [108], [109]. Hence, there is an opportunity to present an analysis that expands on other areas that have employed GMWs besides the ones discussed in this paper.

Moreover, the sample size of articles found and reviewed based on the search procedure is another limitation of the present study. This study reviewed a greater number of articles focused on biomedical engineering or medical

applications since the presented search strategy led to a greater sample of articles focused on that area. Nonetheless, this does not imply that the concept of the WT or CWT has not been used extensively in the other reviewed fields presented in this study. The above highlights applications and fields where GMWs could be used more extensively. Moreover, studies that highlight the areas of opportunity of the GMWs for specific applications or areas can be performed since this paper was mainly centered on providing a general overview of the use of GMWs in the literature and gaps related to their parametrizations.

VII. CONCLUSION AND FUTURE WORK

This study presented a review of the applications of the CWT generated through GMWs. This study's findings reveal that GMWs and the CWT have been used extensively in medical and biomedical engineering applications to perform physiological signal analysis and health monitoring tasks. Furthermore, this signal decomposition technique has also been useful in fluid dynamics, vibration, and systems analysis. Moreover, electrical engineering, geophysics, and communication systems are other fields in which the GMWs have been used to a lesser extent. In addition, it was observed that a frequent use of the CWT and GMWs is for signal classification performed through CNNs, where the scalogram of the CWT is used as input into the CNN. Nevertheless, one of the major drawbacks related to the use of the GMWs is that most of the reviewed studies did not report the values of the parameters of the GMWs, which difficulties the reproduction of the results and their respective analysis.

The parameters of the GMWs used for each field and application were also reviewed and analyzed. It was observed that a common choice for the gamma value is $\gamma = 3$ since, for this value, GMWs approximates the lower-bound of the Heisenberg area (i.e., $A_\psi = 0.5$). Thus, the current uses of this wavelet family have been restricted to a particular region of their parameter space. On the other hand, a reference metric and argumentation related to the adequate selection of beta or time-bandwidth product for a specific signal, system, or process have yet to perform or discussed extensively.

Taking the above into account, the following points are proposed as prospective future research advancements for the use of GMWs and the WT:

- Explore and analyze other regions of the parameter space of the GMWs where the lower-bound of the Heisenberg area is approximated aside from $\gamma = 3$ to compute the CWT.
- A methodology or robust argumentation for the selection of beta (β) or time-bandwidth product (P^2) could be proposed and implemented to determine its adequate choice based on the characteristics of the signal, system, or process that is analyzed.
- An analysis of the optimal selection of the number of filters or voices per octave when computing the CWT through the GMWs and its interaction with the parameters gamma and beta could be performed according to the signal, system, or process characteristics that is been studied.
- There is an opportunity of generating software implementations of the GMWs in other platforms besides MATLAB, such as R, Octave, LabVIEW, or Julia, which could facilitate the reproduction and comparison of the results between different software platforms, applications, and fields.
- The GMWs have been mostly used under the paradigm of the CWT; nevertheless, implementations of GMWs by performing other types of WT-related techniques, such as the discrete wavelet transform or TQWT, can be developed.
- The CWT and GMWs have been primarily used to solve classification tasks through CNNs. However, other types of machine learning or deep learning techniques that can be used with the CWT and GMWs for signal classification problems could be explored. For instance, using recurrent neural networks or generating features from the CWT generated through the GMWs could be employed to train classical machine learning techniques without depending on complex black-box classifiers based on deep learning.

REFERENCES

[1] F. Hlawatsch and F. Auger, *Time-Frequency Analysis* (ISTE). Hoboken, NJ, USA: Wiley, 2013.

[2] R. Brown and P. Hwang, *Introduction to Random Signals and Applied Kalman Filtering With MATLAB Exercises and Solutions*. Hoboken, NJ, USA: Wiley, 1997.

[3] B. Boashash, *Time Frequency Signal Analysis and Processing: A Comprehensive Reference*, 1st ed. Amsterdam, The Netherlands: Elsevier, 2016.

[4] S. L. Brunton and J. N. Kutz, *Dimensionality Reduction and Transforms*. Cambridge, U.K.: Cambridge Univ. Press, 2019, pp. 1–2.

[5] J. Morlet, G. Arens, E. Fourgeau, and D. Glard, "Wave propagation and sampling theory—Part I: Complex signal and scattering in multilayered media," *Geophysics*, vol. 47, no. 2, pp. 203–221, Feb. 1982.

[6] M. S. Manikandan and S. Dandapat, "Wavelet-based electrocardiogram signal compression methods and their performances: A prospective review," *Biomed. Signal Process. Control*, vol. 14, pp. 73–107, Nov. 2014.

[7] J. M. Shapiro, "Embedded image coding using zerotrees of wavelet coefficients," *IEEE Trans. Signal Process.*, vol. 41, no. 12, pp. 3445–3462, Dec. 1993.

[8] Y. Yang, Z. Peng, and W. Zhang, "Parameterised time-frequency analysis methods and their engineering applications: A review of recent advances," *Mech. Syst. Signal Process.*, vol. 119, pp. 182–221, Jan. 2019.

[9] M. Akay, "Wavelets in biomedical engineering," *Ann. Biomed. Eng.*, vol. 23, no. 5, pp. 531–542, Sep. 1995.

[10] H. Witte and M. Wacker, "Time-frequency techniques in biomedical signal analysis," *Methods Inf. Med.*, vol. 52, no. 4, pp. 279–296, 2013.

[11] D. Pasqualotto and M. Zigliotto, "Increasing feasibility of neural network-based early fault detection in induction motor drives," *IEEE J. Emerg. Sel. Topics Power Electron.*, vol. 10, no. 2, pp. 2042–2051, Apr. 2022.

[12] G. Nusev, D. Juričić, M. Gaberšček, J. Moskon, and P. Boškoski, "Fast impedance measurement of li-ion battery using discrete random binary excitation and wavelet transform," *IEEE Access*, vol. 9, pp. 46152–46165, 2021.

[13] V. V. Moca, H. Bârzan, A. Nagy-Dăbâcan, and R. C. Mureşan, "Time-frequency super-resolution with superlets," *Nature Commun.*, vol. 12, no. 1, p. 337, Jan. 2021.

[14] R. Parhizkar, Y. Barbotin, and M. Vetterli, "Sequences with minimal time–frequency uncertainty," *Appl. Comput. Harmon. Anal.*, vol. 38, no. 3, pp. 452–468, May 2015.
[15] L. Durak and O. Arikan, "Short-time Fourier transform: Two fundamental properties and an optimal implementation," *IEEE Trans. Signal Process.*, vol. 51, no. 5, pp. 1231–1242, May 2003.
[16] M. Rhif, A. Ben Abbes, I. Farah, B. Martínez, and Y. Sang, "Wavelet transform application for/in non-stationary time-series analysis: A review," *Appl. Sci.*, vol. 9, no. 7, p. 1345, Mar. 2019.
[17] M. Zamorano, M. J. Gómez Garcia, and C. Castejón, "Selection of a mother wavelet as identification pattern for the detection of cracks in shafts," *J. Vib. Control*, vol. 28, nos. 21–22, pp. 3152–3161, Nov. 2022.
[18] J. M. Lilly and S. C. Olhede, "Generalized Morse wavelets as a superfamily of analytic wavelets," *IEEE Trans. Signal Process.*, vol. 60, no. 11, pp. 6036–6041, Nov. 2012.
[19] T. Guo, T. Zhang, E. Lim, M. López-Benítez, F. Ma, and L. Yu, "A review of wavelet analysis and its applications: Challenges and opportunities," *IEEE Access*, vol. 10, pp. 58869–58903, 2022.
[20] I. Daubechies, "Time-frequency localization operators: A geometric phase space approach," *IEEE Trans. Inf. Theory*, vol. IT-34, no. 4, pp. 605–612, Jul. 1988.
[21] S. C. Olhede and A. T. Walden, "Generalized Morse wavelets," *IEEE Trans. Signal Process.*, vol. 50, no. 11, pp. 2661–2670, Nov. 2002.
[22] Z.-C. Wang, W.-X. Ren, and G. Chen, "Time–frequency analysis and applications in time-varying/nonlinear structural systems: A state-of-the-art review," *Adv. Struct. Eng.*, vol. 21, no. 10, pp. 1562–1584, Jul. 2018.
[23] A. Anwarsha and T. N. Babu, "A review on the role of tunable *Q*-factor wavelet transform in fault diagnosis of rolling element bearings," *J. Vib. Eng. Technol.*, vol. 10, no. 5, pp. 1793–1808, Jul. 2022.
[24] R. Camussi and S. Meloni, "On the application of wavelet transform in jet aeroacoustics," *Fluids*, vol. 6, no. 8, p. 299, Aug. 2021.
[25] A. Rinoshika and H. Rinoshika, "Application of multi-dimensional wavelet transform to fluid mechanics," *Theor. Appl. Mech. Lett.*, vol. 10, no. 2, pp. 98–115, Jan. 2020.
[26] A. Grossmann and J. Morlet, "Decomposition of Hardy functions into square integrable wavelets of constant shape," *SIAM J. Math. Anal.*, vol. 15, no. 4, pp. 723–736, 1984.
[27] S. Mallat, *A Wavelet Tour of Signal Processing: The Sparse Way*. Amsterdam, The Netherlands: Elsevier, 2008.
[28] I. Daubechies, *Ten Lectures on Wavelets*. Philadelphia, PA, USA: Society for Industrial and Applied Mathematics, 1992.
[29] J. M. Lilly. (2021). *jLab: A Data Analysis Package for MATLAB, Version 1.6.5*. [Online]. Available: http://www.jmlilly.net/jmlsoft.html
[30] J. M. Lilly and S. C. Olhede, "On the analytic wavelet transform," *IEEE Trans. Inf. Theory*, vol. 56, no. 8, pp. 4135–4156, Aug. 2010.
[31] J. M. Lilly and S. C. Olhede, "Higher-order properties of analytic wavelets," *IEEE Trans. Signal Process.*, vol. 57, no. 1, pp. 146–160, Jan. 2009.
[32] P. M. Morse, "Diatomic molecules according to the wave mechanics. II. Vibrational levels," *Phys. Rev.*, vol. 34, no. 1, pp. 57–64, Jul. 1929.
[33] W. A. Woyczynski, *A First Course in Statistics for Signal Analysis*. Boston, MA, USA: Birkhäuser, 2011.
[34] X. Yan, D. Yang, Z. Lin, and B. Vucetic, "Significant low-dimensional spectral-temporal features for seizure detection," *IEEE Trans. Neural Syst. Rehabil. Eng.*, vol. 30, pp. 668–677, 2022.
[35] H. Serhal, N. Abdallah, J.-M. Marion, P. Chauvet, M. Oueidat, and A. Humeau-Heurtier, "Overview on prediction, detection, and classification of atrial fibrillation using wavelets and AI on ECG," *Comput. Biol. Med.*, vol. 142, Mar. 2022, Art. no. 105168.
[36] P. Agarwal and S. Kumar, "Electroencephalography-based imagined speech recognition using deep long short-term memory network," *ETRI J.*, vol. 44, no. 4, pp. 672–685, Jun. 2022.
[37] M. P. Wachowiak, R. Wachowiak-Smolíková, M. J. Johnson, D. C. Hay, K. E. Power, and F. M. Williams-Bell, "Quantitative feature analysis of continuous analytic wavelet transforms of electrocardiography and electromyography," *Phil. Trans. Roy. Soc. A, Math., Phys. Eng. Sci.*, vol. 376, no. 2126, Jul. 2018, Art. no. 20170250.
[38] L. G. Weiss, "Wavelet transforms for nonstationary signal processing," *Proc. SPIE*, vol. 3813, pp. 540–550, Oct. 1999.
[39] M. Alafeef and M. Fraiwan, "On the diagnosis of idiopathic Parkinson's disease using continuous wavelet transform complex plot," *J. Ambient Intell. Hum. Comput.*, vol. 10, no. 7, pp. 2805–2815, Jul. 2019.
[40] Y.-H. Byeon, S.-B. Pan, and K.-C. Kwak, "Intelligent deep models based on scalograms of electrocardiogram signals for biometrics," *Sensors*, vol. 19, no. 4, p. 935, Feb. 2019.
[41] R. Cartas-Rosado, B. Becerra-Luna, R. Martínez-Memije, Ó. Infante-Vázquez, C. Lerma, H. Pérez-Grovas, and J. M. Rodríguez-Chagolla, "Continuous wavelet transform based processing for estimating the power spectrum content of heart rate variability during hemodiafiltration," *Biomed. Signal Process. Control*, vol. 62, Sep. 2020, Art. no. 102031.
[42] B. L. Smarr, I. Zucker, and L. J. Kriegsfeld, "Detection of successful and unsuccessful pregnancies in mice within hours of pairing through frequency analysis of high temporal resolution core body temperature data," *PLoS ONE*, vol. 11, no. 7, pp. 1–12, Jul. 2016.
[43] A. D. Grant, M. Newman, and L. J. Kriegsfeld, "Ultradian rhythms in heart rate variability and distal body temperature anticipate onset of the luteinizing hormone surge," *Sci. Rep.*, vol. 10, no. 1, p. 20378, Nov. 2020.
[44] L. Wiklendt, S. J. H. Brookes, M. Costa, L. Travis, N. J. Spencer, and P. G. Dinning, "A novel method for electrophysiological analysis of EMG signals using MesaClip," *Frontiers Physiol.*, vol. 11, p. 484, Jun. 2020.
[45] A. E. Farah Malik, S. Barin, and M. E. Yüksel, "Accurate classification of heart sound signals for cardiovascular disease diagnosis by wavelet analysis and convolutional neural network: Preliminary results," in *Proc. 28th Signal Process. Commun. Appl. Conf. (SIU)*, Oct. 2020, pp. 1–4.
[46] S. C. Mohonta, M. A. Motin, and D. K. Kumar, "Electrocardiogram based arrhythmia classification using wavelet transform with deep learning model," *Sens. Bio-Sensing Res.*, vol. 37, Aug. 2022, Art. no. 100502.
[47] P. Zontone, A. Affanni, A. Piras, and R. Rinaldo, "Exploring physiological signal responses to traffic-related stress in simulated driving," *Sensors*, vol. 22, no. 3, p. 939, Jan. 2022.
[48] G. Campi and A. Bianconi, "Periodic recurrent waves of COVID-19 epidemics and vaccination campaign," *Chaos, Solitons Fractals*, vol. 160, Jul. 2022, Art. no. 112216.
[49] C. E. Davila, D. X. Wang, M. Ritzer, R. Moran, and B. C. Lega, "A control-theoretical system for modulating hippocampal gamma oscillations using stimulation of the posterior cingulate cortex," *IEEE Trans. Neural Syst. Rehabil. Eng.*, vol. 30, pp. 2242–2253, 2022.
[50] B. L. Smarr, K. Aschbacher, S. M. Fisher, A. Chowdhary, S. Dilchert, K. Puldon, A. Rao, F. M. Hecht, and A. E. Mason, "Feasibility of continuous fever monitoring using wearable devices," *Sci. Rep.*, vol. 10, no. 1, p. 21640, Dec. 2020.
[51] S. Suwansawang and D. M. Halliday, "Wavelet-based method for coherence analysis with suppression of low frequency envelope modulation in non-stationary signals," in *Proc. 8th Int. Electr. Eng. Congr. (iEECON)*, Mar. 2020, pp. 1–4.
[52] M. Finžgar and P. Podržaj, "A wavelet-based decomposition method for a robust extraction of pulse rate from video recordings," *PeerJ*, vol. 6, Nov. 2018, Art. no. e5859.
[53] G. Riches, R. Martinuzzi, and C. Morton, "Proper orthogonal decomposition analysis of a circular cylinder undergoing vortex-induced vibrations," *Phys. Fluids*, vol. 30, no. 10, Oct. 2018, Art. no. 105103.
[54] Y. Liu, X. Jiang, C. Lee, and H. Hu, "An experimental study on the spatiotemporal evolution of sand waves/ripples in turbulent boundary layer airflow," *Phys. Fluids*, vol. 32, no. 6, Jun. 2020, Art. no. 063304.
[55] H. B. Yates, M. W. Tufts, and T. J. Juliano, "Analysis of the hypersonic cross-flow instability with experimental wavenumber distributions," *J. Fluid Mech.*, vol. 883, p. A50, Jan. 2020.
[56] M.-P. Lelong, Y. Cuypers, and P. Bouruet-Aubertot, "Near-inertial energy propagation inside a Mediterranean anticyclonic eddy," *J. Phys. Oceanogr.*, vol. 50, no. 8, pp. 2271–2288, Aug. 2020.
[57] Y. X. Wang, K.-S. Choi, M. Gaster, C. Atkin, V. Borodulin, and Y. Kachanov, "Early development of artificially initiated turbulent spots," *J. Fluid Mech.*, vol. 916, p. A1, Jun. 2021.
[58] Y. X. Wang, K.-S. Choi, M. Gaster, C. Atkin, V. Borodulin, and Y. Kachanov, "Opposition control of turbulent spots," *J. Fluid Mech.*, vol. 943, p. A3, Jul. 2022.
[59] T. Abuhamdia, S. Taheri, and J. Burns, "Laplace wavelet transform theory and applications," *J. Vib. Control*, vol. 24, no. 9, pp. 1600–1620, May 2018.
[60] G. Baldini, R. Giuliani, and F. Geib, "On the application of time frequency convolutional neural networks to road anomalies' identification with accelerometers and gyroscopes," *Sensors*, vol. 20, no. 22, p. 6425, Nov. 2020.

[61] A. Khan, J.-S. Kim, and H. S. Kim, "Damage detection and isolation from limited experimental data using simple simulations and knowledge transfer," *Mathematics*, vol. 10, no. 1, p. 80, Dec. 2021.
[62] G. T. Garro, B. T. Warwick, and C. K. Mechefske, "Analysis of an automobile door closure vibroacoustic response," *J. Vib. Control*, vol. 27, nos. 5–6, pp. 597–611, Mar. 2021.
[63] M. Civera and C. Surace, "Instantaneous spectral entropy: An application for the online monitoring of multi-storey frame structures," *Buildings*, vol. 12, no. 3, p. 310, Mar. 2022.
[64] M. Civera and C. Surace, "An application of instantaneous spectral entropy for the condition monitoring of wind turbines," *Appl. Sci.*, vol. 12, no. 3, p. 1059, Jan. 2022.
[65] S. Mahato and A. Chakraborty, "Sequential clustering of synchrosqueezed wavelet transform coefficients for efficient modal identification," *J. Civil Struct. Health Monit.*, vol. 9, no. 2, pp. 271–291, Apr. 2019.
[66] M. Jin, M. R. W. Brake, and H. Song, "Comparison of nonlinear system identification methods for free decay measurements with application to jointed structures," *J. Sound Vib.*, vol. 453, pp. 268–293, Aug. 2019.
[67] C. Wang, J. Zhang, and H. P. Zhu, "A combined method for time-varying parameter identification based on variational mode decomposition and generalized Morse wavelet," *Int. J. Struct. Stability Dyn.*, vol. 20, no. 7, Jul. 2020, Art. no. 2050077.
[68] J. Yan, S. Laflamme, P. Singh, A. Sadhu, and J. Dodson, "A comparison of time-frequency methods for real-time application to high-rate dynamic systems," *Vibration*, vol. 3, no. 3, pp. 204–216, Aug. 2020.
[69] Y. Zhu, H. Sekiya, T. Okatani, I. Yoshida, and S. Hirano, "Acceleration-based deep learning method for vehicle monitoring," *IEEE Sensors J.*, vol. 21, no. 15, pp. 17154–17161, Aug. 2021.
[70] A. Mitra, Y. Giridharan, and A. Chakraborty, "Wavelet linear quadratic regulator-based gain scheduling for optimal fore-aft vibration control of horizontal axis wind turbine tower using active tuned mass damper," *Struct. Control Health Monit.*, vol. 29, no. 11, Nov. 2022, Art. no. e3055.
[71] A. Lanning, A. E. Zaghi, and T. Zhang, "Applicability of convolutional neural networks for calibration of nonlinear dynamic models of structures," *Frontiers Built Environ.*, vol. 8, Apr. 2022, Art. no. 873546.
[72] L. A. Magrini, M. O. Domingues, E. E. N. Macau, and I. Z. Kiss, "Extraction of slow and fast dynamics of multiple time scale systems using wavelet techniques," *Chaos, Interdiscipl. J. Nonlinear Sci.*, vol. 30, no. 6, Jun. 2020, Art. no. 063139.
[73] S. A. Taher, J. Li, J.-H. Jeong, S. Laflamme, H. Jo, C. Bennett, W. N. Collins, and A. R. J. Downey, "Structural health monitoring of fatigue cracks for steel bridges with wireless large-area strain sensors," *Sensors*, vol. 22, no. 14, p. 5076, Jul. 2022.
[74] B. Joyce, J. Dodson, S. Laflamme, and J. Hong, "An experimental test bed for developing high-rate structural health monitoring methods," *Shock Vib.*, vol. 2018, Jun. 2018, Art. no. 3827463.
[75] A. Abedini-Livari, K. Firuzi, and M. Vakilian, "Distinguishing polymeric insulators PD sources through RF PD measurement," *IET Gener., Transmiss. Distrib.*, vol. 14, no. 21, pp. 4859–4865, Nov. 2020.
[76] O. A. Allan and W. G. Morsi, "A new passive islanding detection approach using wavelets and deep learning for grid-connected photovoltaic systems," *Electr. Power Syst. Res.*, vol. 199, Oct. 2021, Art. no. 107437.
[77] Y. Seyedi, J. Mahseredjian, and H. Karimi, "Impact of fault impedance and duration on transient response of hybrid AC/DC microgrid," *Electr. Power Syst. Res.*, vol. 197, Aug. 2021, Art. no. 107298.
[78] T. McGrew, V. Sysoeva, C.-H. Cheng, C. Miller, J. Scofield, and M. J. Scott, "Condition monitoring of DC-link capacitors using time–frequency analysis and machine learning classification of conducted EMI," *IEEE Trans. Power Electron.*, vol. 37, no. 10, pp. 12606–12618, Oct. 2022.
[79] P. Wang and J. Gao, "Extraction of instantaneous frequency from seismic data via the generalized Morse wavelets," *J. Appl. Geophys.*, vol. 93, pp. 83–92, Jun. 2013.
[80] Z. Wang, J. Gao, P. Wang, and X. Jiang, "The analytic wavelet transform with generalized Morse wavelets to detect fluvial channels in the Bohai bay basin, China," *Geophysics*, vol. 81, no. 4, pp. O1–O9, Jul. 2016.
[81] R. Whitney, "Quantifying near fault pulses using generalized Morse wavelets," *J. Seismol.*, vol. 23, no. 5, pp. 1115–1140, Sep. 2019.
[82] Z. Wang, D. Gao, X. Lei, D. Wang, and J. Gao, "Machine learning-based seismic spectral attribute analysis to delineate a tight-sand reservoir in the Sulige gas field of central Ordos basin, western China," *Mar. Petroleum Geol.*, vol. 113, Mar. 2020, Art. no. 104136.
[83] A. Lurka, G. Mutke, and P. Małkowski, "Dynamic influence of near-source seismic ground motion on underground mine working stability using time-frequency analysis," *Shock Vib.*, vol. 2021, Aug. 2021, Art. no. 9023550.
[84] H. Moriya, "Identification of similar seismic waves using the phase-only correlation function and wavelet transform," *Energies*, vol. 14, no. 15, p. 4527, Jul. 2021.
[85] X. Yuan, D. Tanksley, P. Jiao, L. Li, G. Chen, and D. Wunsch, "Encoding time-series ground motions as images for convolutional neural networks-based seismic damage evaluation," *Frontiers Built Environ.*, vol. 7, p. 52, Apr. 2021.
[86] A. Tahir, J. Ahmad, S. A. Shah, G. Morison, D. A. Skelton, H. Larijani, Q. H. Abbasi, M. A. Imran, and R. M. Gibson, "WiFreeze: Multiresolution scalograms for freezing of gait detection in Parkinson's leveraging 5G spectrum with deep learning," *Electronics*, vol. 8, no. 12, p. 1433, Dec. 2019.
[87] S. Ujan, N. Navidi, and R. J. Landry, "An efficient radio frequency interference (RFI) recognition and characterization using end-to-end transfer learning," *Appl. Sci.*, vol. 10, no. 19, p. 6885, Oct. 2020.
[88] P. Ssekidde, O. Steven Eyobu, D. S. Han, and T. J. Oyana, "Augmented CWT features for deep learning-based indoor localization using WiFi RSSI data," *Appl. Sci.*, vol. 11, no. 4, p. 1806, Feb. 2021.
[89] K. Niu, X. Wang, F. Zhang, R. Zheng, Z. Yao, and D. Zhang, "Rethinking Doppler effect for accurate velocity estimation with commodity WiFi devices," *IEEE J. Sel. Areas Commun.*, vol. 40, no. 7, pp. 2164–2178, Jul. 2022.
[90] W.-Y. Kim and D.-H. Seo, "Radar-based human activity recognition combining range–time–Doppler maps and range-distributed-convolutional neural networks," *IEEE Trans. Geosci. Remote Sens.*, vol. 60, pp. 1–11, 2022.
[91] M. Walenczykowska and A. Kawalec, "Application of continuous wavelet transform and artificial naural network for automatic radar signal recognition," *Sensors*, vol. 22, no. 19, p. 7434, Sep. 2022.
[92] L. Torrey and J. Shavlik, "Transfer learning," in *Handbook of Research on Machine Learning Applications and Trends: Algorithms, Methods, and Techniques*. Hershey, PA, USA: IGI Global, 2010, pp. 242–264.
[93] S. Mallat, "Understanding deep convolutional networks," *Philos. Trans. Roy. Soc. A, Math., Phys. Eng. Sci.*, vol. 374, no. 2065, 2016, Art. no. 20150203.
[94] J. Qin, W. Pan, X. Xiang, Y. Tan, and G. Hou, "A biological image classification method based on improved CNN," *Ecol. Informat.*, vol. 58, Jul. 2020, Art. no. 101093.
[95] Jahandad, S. M. Sam, K. Kamardin, N. N. A. Sjarif, and N. Mohamed, "Offline signature verification using deep learning convolutional neural network (CNN) architectures GoogLeNet Inception-v1 and Inception-v3," *Procedia Comput. Sci.*, vol. 161, no. C, pp. 475–483, Jan. 2019, doi: 10.1016/j.procs.2019.11.147.
[96] A. Krizhevsky, I. Sutskever, and G. E. Hinton, "ImageNet classification with deep convolutional neural networks," *Commun. ACM*, vol. 60, no. 6, pp. 84–90, May 2017.
[97] K. He, X. Zhang, S. Ren, and J. Sun, "Deep residual learning for image recognition," in *Proc. IEEE Conf. Comput. Vis. Pattern Recognit. (CVPR)*, Jun. 2016, pp. 770–778.
[98] G. Huang, Z. Liu, L. Van Der Maaten, and K. Q. Weinberger, "Densely connected convolutional networks," in *Proc. IEEE Conf. Comput. Vis. Pattern Recognit. (CVPR)*, Jul. 2017, pp. 2261–2269.
[99] F. Zhuang, Z. Qi, K. Duan, D. Xi, Y. Zhu, H. Zhu, H. Xiong, and Q. He, "A comprehensive survey on transfer learning," *Proc. IEEE*, vol. 109, no. 1, pp. 43–76, Jan. 2021.
[100] G. James, D. Witten, T. Hastie, and R. Tibshirani, *An Introduction to Statistical Learning*. New York, NY, USA: Springer, 2013.
[101] J. P. Chu and C. T. Kemere, "GhostiPy: An efficient signal processing and spectral analysis toolbox for large data," *eNeuro*, vol. 8, no. 6, pp. 1–19, Nov. 2021.
[102] X. Bei, N. Chen, and S. Zhang, "On the complexity of trial and error," in *Proc. 45th Annu. ACM Symp. Symp. Theory Comput. (STOC)*. New York, NY, USA: Association for Computing Machinery, 2013, pp. 31–40.
[103] Y. Tian, J. Gao, N. Liu, and D. Chen, "Construction of optimal basic wavelet via AIDNN and its application in seismic data analysis," *IEEE Geosci. Remote Sens. Lett.*, vol. 18, no. 7, pp. 1144–1148, Jul. 2021.
[104] P. M. Bentley and J. T. E. McDonnell, "Wavelet transforms: An introduction," *Electron. Commun. Eng. J.*, vol. 6, no. 4, pp. 175–186, Aug. 1994.

[105] K. E. Deane, M. G. K. Brunk, A. W. Curran, M. M. Zempeltzi, J. Ma, X. Lin, F. Abela, S. Aksit, M. Deliano, F. W. Ohl, and M. F. K. Happel, "Ketamine anaesthesia induces gain enhancement via recurrent excitation in granular input layers of the auditory cortex," *J. Physiol.*, vol. 598, no. 13, pp. 2741–2755, Jul. 2020.
[106] O. Kocahan, E. Tiryaki, E. Coskun, and S. Ozder, "Determination of phase from the ridge of CWT using generalized Morse wavelet," *Meas. Sci. Technol.*, vol. 29, no. 3, Feb. 2018, Art. no. 035203.
[107] R. Soulard and P. Carré, "Elliptical monogenic wavelets for the analysis and processing of color images," *IEEE Trans. Signal Process.*, vol. 64, no. 6, pp. 1535–1549, Mar. 2016.
[108] D. Gabriel, D. Cécile, F. Anne, and P. Valérie, "Generalized Morse wavelet frame estimation applied to side-channel analysis," in *Proc. 6th Int. Conf. Frontiers Signal Process. (ICFSP)*, Sep. 2021, pp. 52–57.
[109] K. L. B. L. Xavier and V. K. Nanayakkara, "Development of an early fire detection technique using a passive infrared sensor and deep neural networks," *Fire Technol.*, vol. 58, no. 6, pp. 3529–3552, Nov. 2022.

ERICK AXEL MARTINEZ-RÍOS was born in Mexico City, Mexico, in May 1995. He received the B.S. degree (Hons.) in mechatronics engineering and the M.S. degree (Hons.) in engineering science from the Instituto Tecnológico y de Estudios Superiores de Monterrey, Mexico City, in 2017 and 2022, respectively. He is currently pursuing the Ph.D. degree in engineering science with the Instituto Tecnológico y de Estudios Superiores de Monterrey.

From 2018 to 2020, he worked as a Project Specialist with the Instituto Tecnológico y de Estudios Superiores de Monterrey. During this stay, he worked on research and development projects in the field of robotics. He is the author of four journal articles, one conference paper, and one book chapter. His research interests include signal processing, machine learning, and control theory.

ROGELIO BUSTAMANTE-BELLO was born in Orizaba, Veracruz, in 1965. He received the B.S. degree in electronic instrumentation from the Faculty of Physics and Mathematics, Universidad Veracruzana, Xalapa, Veracruz, the master's degree in electronics and telecommunications from CICESE, Ensenada, Baja California, Mexico, and the Ph.D. degree in telecommunications and electronics from SEPI, Instituto Politécnico Nacional. He has worked for more than 12 years in advanced bioinstrumentation systems, applying them to the driving assistance systems (ADAS) and the development of healthy active spaces (emotional domotics) and exoskeletons regarding the movement of lower limbs and bioinstrumentation systems. He has filed multiple patents with IMPI and WIPO.

SERGIO NAVARRO-TUCH (Member, IEEE) was born in Mexico City, Mexico, in 1990. He received the B.S. degree in mechatronics engineering and the Ph.D. degree in engineering sciences from the Tecnologico de Monterrey, in 2014 and 2018, respectively. He is currently a part of the Computing Intelligence, Mechatronics, and Biodesign Laboratory, Tecnologico de Monterrey. He is also a KNX Scientific Partner. His research interests include domotics with the implementation of emotional analyzing systems with social therapeutic implementations and UX analysis for life quality improvement, the reason for which he became part of the international association dementia friends.

HECTOR PEREZ-MEANA (Life Senior Member, IEEE) received the M.S. degree in electrical engineering from The University of Electrocommunications and the Ph.D. degree in electrical engineering from the Tokyo Institute of Technology, in 1989. In 1991, he was a Visiting Researcher at the Fujitsu Laboratories. From 1992 to 1997, he was a Professor at the Electrical Engineering Department, Metropolitan Autonomous University, Mexico. He was the Dean of the Graduate and Research Section, IPN, from 2006 to 2010, and from 2016 to 2019, where he is currently a Professor with the Mechanical and Electrical Engineering Department. His research interests include adaptive systems, signal and image processing, pattern recognition, and information security.